SECOND SOUND ATTENUATION IN A LIQUID HELIUM COUNTERFLOW JET

Thesis by

Glenn A. Laguna

In Partial Fulfillment of the Requirements

For the Degree of

Doctor of Philosophy

California Institute of Technology

Pasadena, California

1975

(Submitted March 10, 1975)

ACKNOWLEDGEMENTS

It is a great pleasure to acknowledge all of the people who made this work possible. In particular, I would like to thank my adviser and friend, Professor Hans Wolfgang Liepmann for his advice and encouragement. Drs. James E. Broadwell and Paul Dimotakis have also contributed many helpful suggestions, and the help of Drs. Harris A. Notarys and David Palmer of Low Temperature Physics was indispensible for the thin film fabrication.

The author also wishes to thank Mrs. Betty Wood for her help with the figures and Mrs. Jacquelyn Beard for typing the manuscript and contributing her good humor.

Lastly, I would like to thank the graduate students of GALCIT for leaving the experimental apparatus alone long enough for me to take some measurements. The initial phase of this work was supported by the Alfred P. Sloan Foundation. The final phase of the work was supported by the Air Force Office of Scientific Research.

ABSTRACT

The attenuation of a beam of high frequency second sound traversing a counterflow jet in liquid helium has been measured in the temperature range 1.6 to 2.06°K. Combined use of thin film superconducting thermometers with specially developed low noise amplifiers allowed a temperature resolution of better than one part in 10^8 °K. The additional attenuation due to the jet was found to be less than 10 percent of the predicted value using the theory of mutual friction in a supercritical counterflow, and consistent with the result of earlier temperature gradient and ion beam attenuation measurements.

TABLE OF CONTENTS

TABLE OF CONTENTS (cont.)

I. INTRODUCTION

Liquid helium below the λ-point has been perhaps the most closely scrutinized of all fluids because of its unique position as a fluid whose behavior on a macroscopic scale is governed by quantum mechanical effects. Despite this intensive study, the experimental investigation of the hydrodynamics of liquid helium has been extremely limited, and many of the interesting phenomena observed in classical fluids remain unstudied. Although it is now agreed that the linearized two-fluid equations are accurate in the proper limit, the nonlinear phenomena of shock waves and turbulence have just recently begun to be studied. For example, although Osborne (Ref. 1) in 1951, and Dessler and Fairbank (Ref. 2) in 1956, measured finite amplitude effects in second sound (temperature or entropy waves), shock waves were not observed in liquid helium until the work of Cummings in 1973 (Ref. 3). Turbulence in both the superfluid and normal fluid has often been invoked as an explanation for various observed phenomena in liquid helium, yet no experiments have measured any random fluctuating quantities. In Vinen's (Ref. 4) model of the Gorter-Mellink force the fact that the superfluid is supposedly turbulent is almost irrelevant. Vinen does not introduce any stochastic functions or averaging into his model. There can be no doubt about the need to look closely at these effects of nonlinearity.

The present investigation is third in a group of studies which deals with another hydrodynamic problem. With few exceptions, the experiments on the fluid mechanics of liquid helium have

been on confined flows, i.e., capillaries or wider channels. While this type of geometry is advantageous in the investigation of critical velocities, it is not a clean situation hydrodynamically because there is no way to separate the flow properties from the boundary conditions at the walls, and these boundary conditions are not yet known with certainty (see Ref. 5). The two previous experiments (Ref. 6, 7), as well as the present one, have been concerned with nozzles and jets in liquid helium. The jet provides a flow geometry without walls, thus separating the flow properties from the boundary conditions. As it is unlikely that any applications of liquid helium as a coolant will use narrow capillaries, it is essential to know the heat transfer characteristics of the bulk fluid for technological purposes.

This experiment is a study of the counterflow jet similar to the jet shown in Figure I. 1. The jet is produced by thermal counterflow or internal convection and is supercritical in the sense that at the orifice the heat flux is high enough to cause a breakdown of the simple two-fluid model. For supercritical counterflow in a channel, the temperature difference between the hot and cold ends of the channel is proportional to the cube of the heat flux, with a constant of proportionality dependent only on the bath temperature and not on geometry. This empirical result prompted Gorter and Mellink (Ref. 8) to append mutual friction terms to the two-fluid equations. This accounts for the temperature gradient and produces an additional linear attenuation of second sound. However, the geometry independent temperature gradient is not

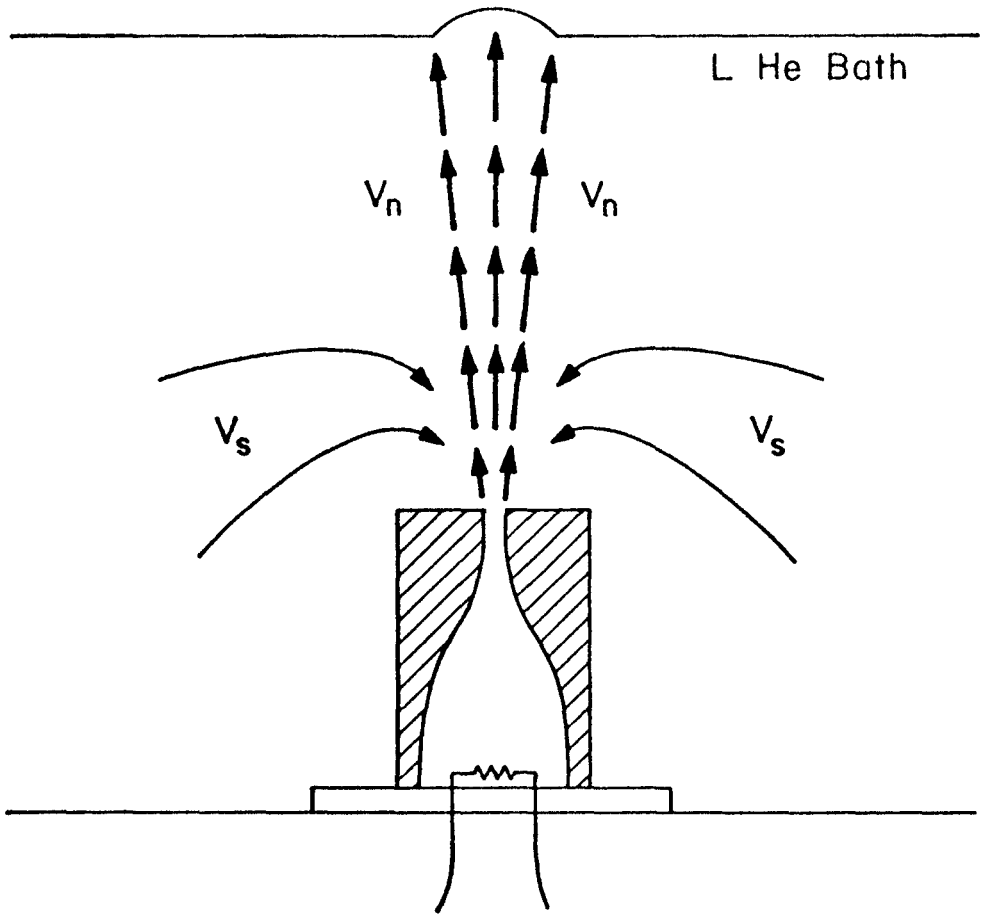

Figure I. 1. The counterflow jet

consistent with the investigation of Dimotakis and Broadwell (Ref. 7) who measured the temperature gradient along the axis of the jet and found that the gradient disappeared within one jet diameter of the orifice. If the jet remains collimated, as measured by Kapitza (Ref. 9), and if the superfluid is not entrained by the normal fluid (which was shown by Dimotakis to be improbable), then the mutual friction idea must either be modified or abandoned. Additional details of the experiments and mutual friction theory are provided in Chapter II.

In the present work a beam of high frequency second sound was propagated transverse to the jet, and the additional attenuation as a function of heat flux at the orifice was measured. Zero additional attenuation would be consistent with the Dimotakis and Broadwell experiment and would be a further indication of the geometry dependence of mutual friction. The other extreme would be a measurement of the full attenuation predicted by the Gorter-Mellink force.

An additional goal of this research was to develop a simple system for the detection of high frequency second sound specifically for use in flow investigations of liquid helium. Even under the most ideal conditions and with maximum power input to the second sound emitter, the amplitude of a 1 MHz wave one centimeter from the emitter would be 10^{-5} to 10^{-7} ^{o}K, and this could be substantially reduced by the Kapitza boundary effect. Recent developments in electronic spectral analysis equipment have made a simple detection scheme feasible. This will permit the extensive use of

high frequency second sound as a local probe for heat transfer studies in liquid helium.

REFERENCES

1. D. V. Osborne, Proc. Phys. Soc. (London) 64, 114 (1951).
2. A. J. Dessler and W. M. Fairbank, Phys. Rev. 104, 6 (1956).
3. J. C. Cummings, Ph. D. Thesis, California Institute of Technology (1973).
4. W. F. Vinen, Proc. Roy. Soc. (London) 242, 493 (1957).
5. C. C. Lin, Liquid Helium, editor Careri (Academic Press, New York, 1963) page 93.
6. J. E. Broadwell and H. W. Liepmann, Phys. Fluids 12, 1533 (1969).
7. P. E. Dimotakis and J. E. Broadwell, Phys. Fluids 16, 1787 (1973).
8. C. J. Gorter and J. H. Mellink, Physica 15, 285 (1949).
9. P. L. Kapitza, J. Phys. USSR 4, 181 (1941).

II. THE TWO-FLUID MODEL AND MUTUAL FRICTION

II. A. Review of the Two-Fluid Model

The hydrodynamics of liquid helium below the λ-point can be described by a two-fluid model suggested by Landau (Ref. 1) and Tisza (Ref. 2). The motion of the liquid is considered to consist of the motion of two interpenetrating but noninteracting fluids, each described by its own density and velocity fields. The superfluid has a density ρ_s and velocity $\vec{v}_s$. As the absolute zero of temperature is approached, all the fluid becomes superfluid, i.e., $\rho_s \to \rho$ as $T \to 0$. Therefore, the superfluid carries no entropy and must flow reversibly without viscous dissipation. As a consequence, Landau postulated that the velocity field of the superfluid must be irrotational. The normal fluid with density ρ_n and velocity v_n is normal in the sense that it has a viscosity η and carries all the entropy.

With the above understanding the equations of motion for the two fluids can be derived (see Ref. 3). The total density is the sum of the superfluid plus normal fluid densities, and the mass flux is the sum of the superfluid and the normal fluid mass fluxes, i.e.,

$$\rho = \rho_s + \rho_n \qquad \vec{j} = \rho\vec{v} = \rho_s\vec{v}_s + \rho_n\vec{v}_n \quad . \qquad (1)$$

Thus the continuity equation can be written in a way identical to an ordinary fluid,

$$\frac{\partial\rho}{\partial t} + \nabla \cdot \rho\vec{v} = 0 \quad . \qquad (2)$$

The momentum equation is also a straightforward generalization. Neglecting viscous dissipation it can be written simply as

$$\frac{\partial j_i}{\partial t} + \frac{\partial}{\partial x_k} \pi_{ik} = 0 \qquad \pi_{ik} = \rho_n v_{ni} v_{nk} + \rho_s v_{si} v_{sk} + p \delta_{ik} . \tag{3}$$

Since the normal fluid carries all the entropy, the entropy flux must be $\rho s \vec{v}_n$ where s is the entropy per unit mass. Neglecting sources of entropy we have

$$\frac{\partial \rho s}{\partial t} + \nabla \cdot (\rho s \vec{v}_n) = 0 \quad . \tag{4}$$

Lastly one must consider how the superfluid moves. As it is presumed irrotational, its convective derivative can be derived from a scalar potential, i.e.,

$$\frac{\partial \vec{v}_s}{\partial t} + \nabla \left(\frac{v_s^2}{2} + \mu \right) = 0 \quad . \tag{5}$$

Arguments of Galilean invariance identify μ with the chemical potential per unit mass (see Ref. 4). Upon rearrangement and inclusion of the normal fluid viscosity the equations appear as in Table II. 1 where they have been summarized for easy reference.

There are two consequences of the equations of motion which are of particular importance to the present work. First, through the chemical potential term in the equation for the superfluid, a temperature gradient acts as a driving force on the superfluid causing it to change its velocity. Thus, in the absence of walls, ordinary heat conduction is excluded as a mechanism of heat transport. Instead it is replaced by the highly efficient heat

Table II. 1

Two-Fluid Equations of Motion

Mass Conservation $$\frac{\partial \rho}{\partial t} + \nabla \cdot \rho \vec{v} = 0$$

Momentum Conservation

$$\frac{\partial}{\partial t}(\rho \vec{v}) + \nabla \cdot \left(\rho \vec{v}\vec{v} + \frac{\rho_s \rho_n}{\rho} \vec{w}\vec{w}\right) + \nabla p = \eta \nabla^2 \left(\vec{v} + \frac{\rho_s}{\rho} \vec{w}\right)$$

Entropy Conservation

$$\frac{\partial \rho s}{\partial t} + \nabla \cdot (\rho s v_n) = \frac{\varkappa (\nabla T)^2}{T^2}$$

Superfluid

$$\frac{\partial \vec{v}_s}{\partial t} + \nabla \left(\frac{v_s^2}{2} + \mu\right) = 0$$

where $\vec{v} = \rho_n \vec{v}_n + \rho_s \vec{v}_s$ $\qquad \vec{w} = \vec{v}_n - \vec{v}_s$

$\varkappa$ = thermal conductivity $\qquad \eta$ = bulk viscosity.

transfer method of thermal counterflow or internal convection, which is an isothermal, convective heat transport (see Ref. 5). The heat flux vector is the product of the entropy flux and the absolute temperature, i. e.,

$$\vec{q} = \rho s T \vec{v}_n \tag{6}$$

If there are solid boundaries a temperature gradient proportional to the heat flux can be maintained owing to the viscous interaction of the normal component with the walls. For a channel of constant diameter this is found to be

$$\frac{\partial T}{\partial x} = - \frac{G\eta_n}{(\rho s)^2 T} q_x = - a q_x \tag{7}$$

where G is a geometry-dependent constant.

A second consequence of the two-fluid equations is the type of wave motion which the liquid helium will support (see Ref. 6). If the two-fluid equations are linearized and a wave solution is substituted for the superfluid and normal fluid velocities, and the perturbation parts of the pressure and temperature,

$$p = p_o + p' e^{i\omega (t - \frac{x}{u})} \qquad T = T_o + T' e^{i\omega (t - \frac{x}{u})} ,$$

one gets a quartic characteristic polynomial for the phase velocity. Upon neglecting the coefficient of thermal expansion, which is small for all liquids and anomalously small for liquid helium, the quartic separates into two quadratics giving the two velocities

$$u_1^2 = \frac{\partial p}{\partial \rho} \qquad u_2^2 = \frac{T s^2 \rho_s}{c \rho_n} . \tag{8}$$

Through an analysis due to Lifschitz (Ref. 7) the physical nature of these waves becomes clear. The speed u_1 is associated with a pressure wave with the temperature remaining constant to the approximation that β, the coefficient of thermal expansion, can be neglected. The superfluid and normal fluid oscillate in phase so this mode is identical to sound propagation in ordinary fluids. Further consideration shows that this oscillation, which is called first sound, corresponds more to isentropic than isothermal conditions.

The other wave speed, u_2, is associated with a non-dispersive temperature or entropy wave. The superfluid and normal fluid oscillate out of phase in a way that the mass flux equals zero, i.e.,

$$\vec{v_s} = - \rho_n/\rho_s \vec{v_n} \quad .$$

The pressure and density remain constant to first order in β. These temperature waves are unique to liquid helium and have no relation to the highly damped temperature waves in a thermally conducting medium which die out within one thermal wavelength.

This new wave motion, called second sound for historical reasons, was predicted first by Tisza's two-fluid theory and discovered experimentally by Peshkov in 1944 (Ref. 8). Because the coupling to pressure is of order β, second sound is most efficiently excited by a heater rather than a vibrating plate, and a sensitive thermometer is needed for detection.

As a unique property of liquid helium, second sound has

been extensively studied. The attenuation coefficient of second sound, which is usually denoted by α, was derived by Khalatnikov (Ref. 9) in his consideration of the kinetic coefficients of liquid helium. This was measured by Hanson and Pellam (Ref. 10). Their frequencies extended into the 100 kHz range. Perhaps the most dramatic demonstration of the wave nature of second sound was the work of Mercereau, Notarys, and Pellam (Ref. 11). Using frequencies up to 600 kHz they measured the diffraction of second sound from a heater which consisted of an array of equally spaced parallel elements. In a later work, Notarys (Ref. 12) measured the speed and attenuation of second sound with frequencies up to 25 MHz. Using a resonance technique, Notarys found that even at these high frequencies the speed and attenuation were the same as at lower frequencies. A similar resonance technique has been used in this investigation but with greatly simplified electronics.

II. B. Experiments Motivating the Present Research

Despite the successes of the two-fluid model, the equations, as has been remarked by C. T. Lane (Ref. 13), were proposed on the basis of a specific set of experiments and it is not unlikely that they will have to be modified in the course of time. Some of the recent experiments and the modifications to the two-fluid model which they suggest are considered in this section.

Equation (7) for the temperature gradient in a channel can be integrated, providing the coefficient a(T) is reasonably constant (small temperature difference), to give

$$\Delta T = -\ell a q \tag{9}$$

for the temperature difference between the hot and cold ends of a channel in pure counterflow with no net mass flux. This expression was verified for small heat fluxes by Keesom (Ref. 14), but as the heat flux is increased a critical heat flux is reached beyond which the experimentally determined relation between the temperature difference and the heat flux is

$$\Delta T = -\ell \left(aq + bq^3\right) \quad .$$

To account for the cubic dependence of the temperature difference on the heat flux, Gorter and Mellink (Ref. 15) in 1949 proposed appending mutual friction terms to the two-fluid equations. The frictional force was proportional to the cube of the relative velocity of the superfluid and normal fluid, and given by the expression

$$\vec{F}_{sn} = -A \rho_s \rho_n w^2 \vec{w} \qquad \vec{w} = \vec{v}_n - \vec{v}_s \quad . \tag{10}$$

The equations of motion become

$$\frac{\partial \vec{v}_s}{\partial t} + \nabla \left(\frac{v_s^2}{2} + \mu\right) = A \rho_n w^2 \vec{w} \tag{11}$$

$$\frac{\partial \vec{v}_n}{\partial t} + (\vec{v}_n \cdot \nabla)\, \vec{v}_n + \frac{1}{\rho} \nabla p = \frac{\eta_n}{\rho_n} \nabla^2 \vec{v}_n - \frac{\rho_s}{\rho_n} s \nabla T - A \rho_s w^2 \vec{w} \quad . \tag{12}$$

These equations give a temperature gradient in the supercritical region

$$\nabla T = - aq - b(T)\, q^3 \qquad b(T) = \frac{A\rho_n}{s(\rho_s sT)^3} \quad . \qquad (13)$$

Note that $b(T)$ is independent of the size or shape of the channel. This law seems to apply to wide channels over a wide range of heat fluxes and channel dimensions. The coefficient A was measured by Vinen (Ref. 16) and found to be temperature dependent, but only very weakly dependent on the size of the channel.

On the basis of his experimental observations Vinen proposed a mechanism for the mutual friction force (Ref. 16). According to Vinen, the critical relative velocity was representative of a transition to a turbulent state of the superfluid. This turbulent state is characterized by a tangled mass of quantized vortex lines and is roughly analogous to the random fluctuations in the vorticity of a turbulent classical fluid, but with circulation around each vortex core quantized, as suggested by Onsager (Ref. 18) and Feynman (Ref. 19). The mutual friction resulted from the interaction of the excitations which make up the normal fluid with the tangled mass of vortices. Using dimensional analysis and frequent appeals to classical fluid mechanics, Vinen was able to extract the essential dependence of the Gorter-Mellink force on the relative velocity.

Although intuitively appealing, the idea of mutual friction does not appear applicable in all situations where there is a relative velocity. Temperature difference measurements in a channel

where $\vec{v}_s$ and $\vec{v}_n$ could be varied independently (Refs. 20 and 21) show a more complicated dependence on the velocities than can be expressed as a simple function of their difference. To explain these experiments and others, more friction terms were added to the equations of motion; however, the predictive value of Vinen's model is lost and its physical basis somewhat open to question since it relies heavily on geometry independence. One cannot tell a priori which mutual friction terms should be added to describe a flow situation. Still, the Gorter-Mellink law provides results in excellent agreement with pure counterflow in wide channels.

To further investigate the validity of the equations of motion with the Gorter-Mellink force appended, Dimotakis and Broadwell (Ref. 22) measured the temperature gradient in a counterflow jet. In 1941 Kapitza (Ref. 23) observed that a well-defined, collimated jet emerged from the mouth of a counterflow channel and persisted for many channel diameters downstream. That the jet did not spread appreciably was observed by measuring the deflection of a vane moved across the jet. The two-fluid model would identify the effluent as normal fluid while the orifice must represent a sink for the superfluid. Consideration of the superfluid and normal fluid streamlines shows that the jet is a region of high relative velocity extending far into the fluid away from solid boundaries. If the mutual friction is truly a volume force independent of the walls, a temperature gradient should be observed extending all the way to the free surface of the liquid.

Dimotakis and Broadwell measured the temperature gradient

by traversing a small carbon thermometer along the axis of the jet from inside the chamber to well outside the chamber into the free fluid. The startling result was that the temperature gradient was confined to the vicinity of the orifice and disappeared completely within one diameter of the orifice. Note, however, that this result is not at all unusual if one thinks in terms of the analogy between temperature in a counterflow jet and pressure in an ordinary jet. For the classical jet there is no mechanism for the support of a downstream pressure gradient.

A simple explanation, consistent with mutual friction, is that $\vec{w} = 0$ in the jet; i.e., the superfluid is entrained by the normal fluid and so there is no relative velocity. This explanation was considered untenable by Dimotakis (Ref. 24) for the following reason. Let $T(x)$ be the measured temperature at a distance x from the orifice along the axis of the jet. One can form a dimensionless variable $(T(x) - T_\infty)/\Delta T$ where T_∞ is the bath temperature and ΔT is the difference between the chamber and bath temperatures. If this dimensionless temperature is plotted against x, the resulting profile is self-similar for all heat fluxes and bath temperatures (see Ref. 22, Figure 15). The normal fluid would have to entrain the superfluid while $\vec{v}_s$ varies over three orders of magnitude in order to produce this similarity with $\vec{w} = 0$. In summary, the jet represents a region of high relative velocity with no temperature gradient and is therefore inconsistent with a geometry independent mutual friction. This appears to be a significant failure of the Vinen model for supercritical counterflow.

In 1968 another experiment involving counterflow through an orifice was done by Careri, Cerdonio, and Dupré (Ref. 25). This time the observation was by means of a negative ion trapping. Negatively charged ions in liquid helium had been observed to be trapped on the superfluid vortex lines (for explanation see Donnelly, Ref. 26), so that the attenuation of a negative ion beam is a direct measure of the amount of vorticity in the superfluid. The experimenters mounted diodes, each consisting of an ion source and detector, on both sides of an orifice. The experiment consisted of measuring the ion current as a function of the heat flux through the orifice. At a critical heat current they observed a sharp increase in the attenuation of the ion beam in the diode on the normal fluid downstream side (hereafter called simply downstream side) of the orifice with no change in attenuation in the upstream diode. The temperature difference across the orifice was also monitored at the same time. The change in attenuation of the ion beam occurred while the temperature difference was still linear in the heat flux.

The interpretation of this result was that vortex lines created at the orifice interact with the normal fluid and are observed on the downstream side. Normal fluid turbulence could not play an important role since one would then observe a temperature independent Reynolds number for the transition using the normal fluid velocity at the critical heat flux. Although this experiment again suggests entrainment of the superfluid, the interpretation is not wholly convincing. The first objection is that the diodes are mounted symmetrically and close to the orifice, but because of the small size

of the orifice these are still 50 diameters away from the exit plane. Thus the diode on the downstream side is in a region of high v_n while the upstream diode is in a region where $v_n \simeq 0$. Since the vortices are part of the superfluid it is unclear why they should all move with the normal fluid. One would expect only a fraction of the superfluid vortices to be entrained, depending on v_n. Thus it is still unclear why the upstream diode saw no attenuation of the beam.

In view of the Vinen model of mutual friction and the observation by Careri of superfluid vorticity downstream of the orifice even at small heat fluxes, one cannot simply explain the temperature gradient in the Dimotakis and Broadwell experiment. For this reason the present research was undertaken. It is found from the equations of motion with the Gorter-Mellink terms that mutual friction causes an additional linear attenuation of second sound given by

$$e^{-(\Delta\alpha)x} \qquad \Delta\alpha = \frac{A\rho}{2u_2} w^2 \quad . \tag{14}$$

This has been verified by Vinen for pure counterflow in wide channels and interpreted as the scattering of the normal fluid quanta in second sound by the quantized vortices in the turbulent superfluid. In the present experiment an emitter and detector for second sound were placed in a Fabry-Perot resonator configuration on the normal fluid downstream side of the jet. A second sound beam propagated transverse to the jet in a way similar to the ion beam of Ref. 25. The basic experiment consisted of measuring

the attenuation of the second sound beam as a function of the heat flux in the jet. If, as observed by Kapitza and Dimotakis, the jet does not spread, then zero additional attenuation would indicate again that the Gorter-Mellink force must turn itself off outside the jet. Thus zero additional attenuation would be consistent with the results of Dimotakis and Broadwell. This was the expected result. If attenuation of the second sound was observed, this would confirm Careri's measurement and could be compared to Vinen's data for wide channels as a test of the geometry independence of the Gorter-Mellink force.

REFERENCES

1. L. D. Landau, J. Phys. USSR 5, 71 (1941).
2. L. Tisza, Nature 141, 913 (1938).
3. L. D. Landau and E. M. Lifschitz, Fluid Mechanics, (Pergamon Press, London, 1959), pages 510-517.
4. Ibid. page 513.
5. F. London, Superfluids vol. 2, (Dover, New York, 1954), pages 155-164.
6. L. D. Landau and E. M. Lifschitz, Fluid Mechanics, (Pergamon Press, London, 1959), pages 517-522.
7. Ibid. page 519.
8. V. Peshkov, J. Phys. USSR 10, 389 (1946)
9. I. M. Khalatnikov, Introduction to the Theory of Superfluidity, (Benjamin, New York, 1965), pages 78-80.

10. W. B. Hanson and J. R. Pellam, Phys. Rev. 95, 321 (1954).

11. J. Mercereau, H. Notarys, and J. R. Pellam, Proceedings of the Eighth International Conference on Low Temperature Physics. (Toronto, 1960), page 552.

12. H. A. Notarys, Ph. D. Thesis, California Institute of Technology (1964).

13. C. T. Lane, Superfluid Physics (McGraw-Hill, New York, 1962).

14. W. A. Keesom and A. P. Keesom, Physica 3, 359 (1936).

15. C. J. Gorter and J. H. Mellink, Physica 15, 285 (1949).

16. W. F. Vinen, Proc. Roy. Soc. A 240, 114 (1957).

17. W. F. Vinen, Proc. Roy. Soc. A 242, 493 (1957).

18. L. Onsager, Nuovo Cimento 6, 249 (1949).

19. R. P. Feynman, Progress in Low Temp. Physics, vol. 1, (North Holland, Amsterdam, 1955).

20. H. C. Kramers, Superfluid Helium, editor J. F. Allen (Academic Press, New York, 1966) page 199.

21. G. Van Der Heijden, W. J. P De Voogt, and H. C. Kramers, Physica 59, 473 (1972).

22. P. E. Dimotakis and J. E. Broadwell, Phys. Fluids 16, 1787 (1973).

23. P. L. Kapitza, J. Phys. USSR 4, 181 (1941).

24. P. E. Dimotakis, Ph. D. Thesis, California Institute of Technology (1972) page 24.

25. G. Careri, M. Cerdonio, and F. Dupré, Phys. Rev. 167, 233 (1968).

26. R. J. Donnelly, Experimental Superfluidity, (Univ. of Chicago Press, Chicago, 1967), pages 172-207.

III. EXPERIMENTAL APPARATUS

III. A. Counterflow Jet

The counterflow jet is shown in Figure III. 1. It is constructed of lucite with a wall thickness of 1/8 inch. The heat flux through the walls is then under one percent of the total heat flux. The heater at the base of the wide chamber is 25 ohms and is constructed of .005 inch Evanohm wire. Uniform heat distribution over the bottom of the channel was insured by potting the heater in Cerelow, a low melting point alloy similar to Wood's metal.

The orifice is a slit 1/16 inch wide and 1/4 inch long. It is the only region of high heat flux. This shape was chosen for easier alignment of the second sound beam with the jet, while the total area was dictated by the desire to produce heat fluxes comparable to previous experiments and still be able to maintain the bath temperature within the required limits.

III. B. Second Sound Equipment

III. B. 1 Emitter and Detector

The second sound emitter and detector are shown in Figure III.2. The emitter was a gold film less than 100 Å thick and $\frac{1}{2}cm^2$ with 1500Å thick copper leads evaporated under high vacuum onto a glass microscope slide. Electrical contact to the copper was made with indium solder and a drop of silver print paint. The resistance of the emitter was kept very close to 50 ohms at $4.2^{o}K$ to match the impedance of the subminiature coax, thereby reducing second harmonic generation. Second sound was generated by Joule

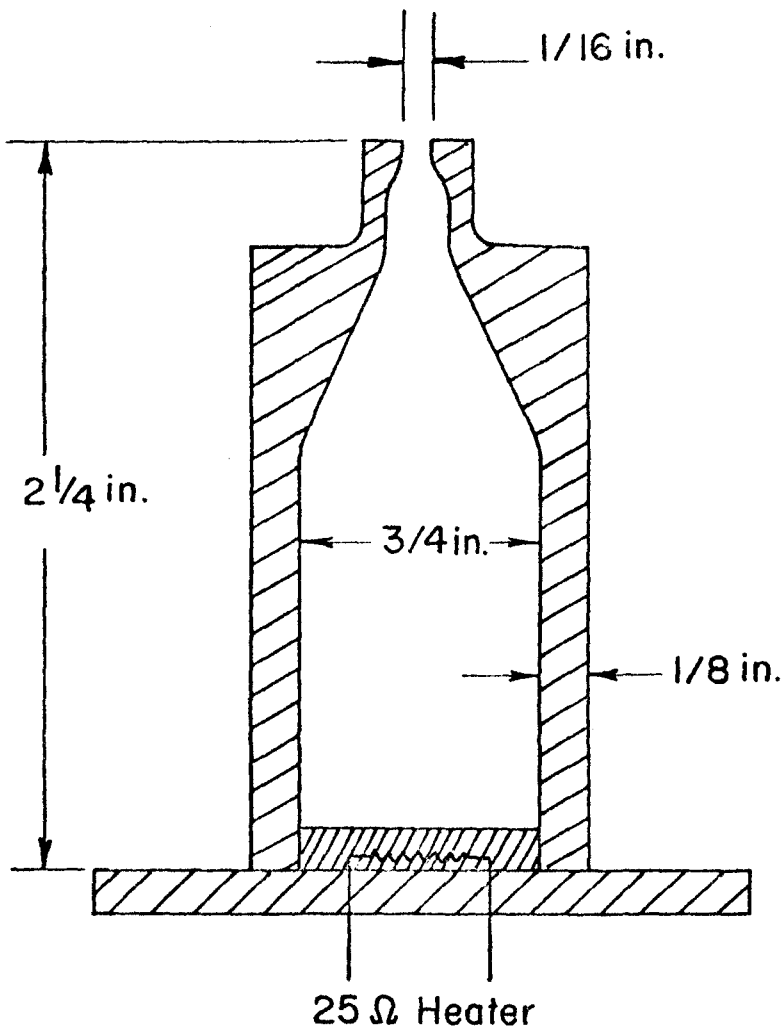

Figure III. 1. Design details of the counterflow jet used in the present experiments.

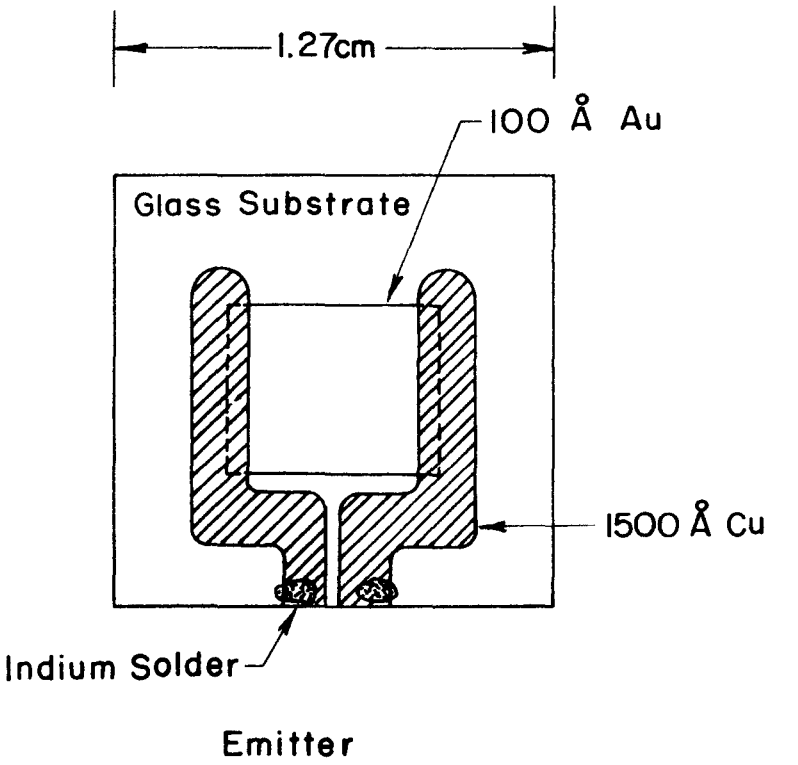

Figure III. 2. Second sound emitter and detector.

heating of the resistive gold film at a frequency $\frac{\omega}{2}$.

A superconducting thin film biased on its transition temperature served as the second sound detector. Typical detector transition curves are shown in Figure III. 3. When the film is fed with a constant current the second sound temperature fluctuations cause a fluctuating resistance of the film and therefore an oscillating voltage drop across it. The films were approximately 1000Å of tin on 250Å of gold. Leads are 1500Å of pure tin which has a transition temperature of 3.72°K and therefore is not sensitive to the temperature fluctuations of second sound. The sensitive area is the one millimeter square flag-shaped region in the center. Fabrication details are supplied in Appendix A.

The basic transition temperature of the film was set by the ratio of tin to gold, but this transition could be lowered by means of a magnetic field as seen in Figure III. 3. In this way one film served as a detector over a wide temperature range. The deviation from linearity of the resistance versus temperature curve in the center of the transition is less than one percent. By optimizing the bias current the detector efficiency, $I_o \frac{dR}{dT}$, could be made as high as 0.6 Volts/°K.

III. B. 2 Second Sound Cell

The second sound cell served the dual purposes of holding the emitter and detector parallel and supporting the magnet which biased the detector. The assembled cell is shown in Figure III. 4. It was machined entirely out of Type 304 stainless steel and has

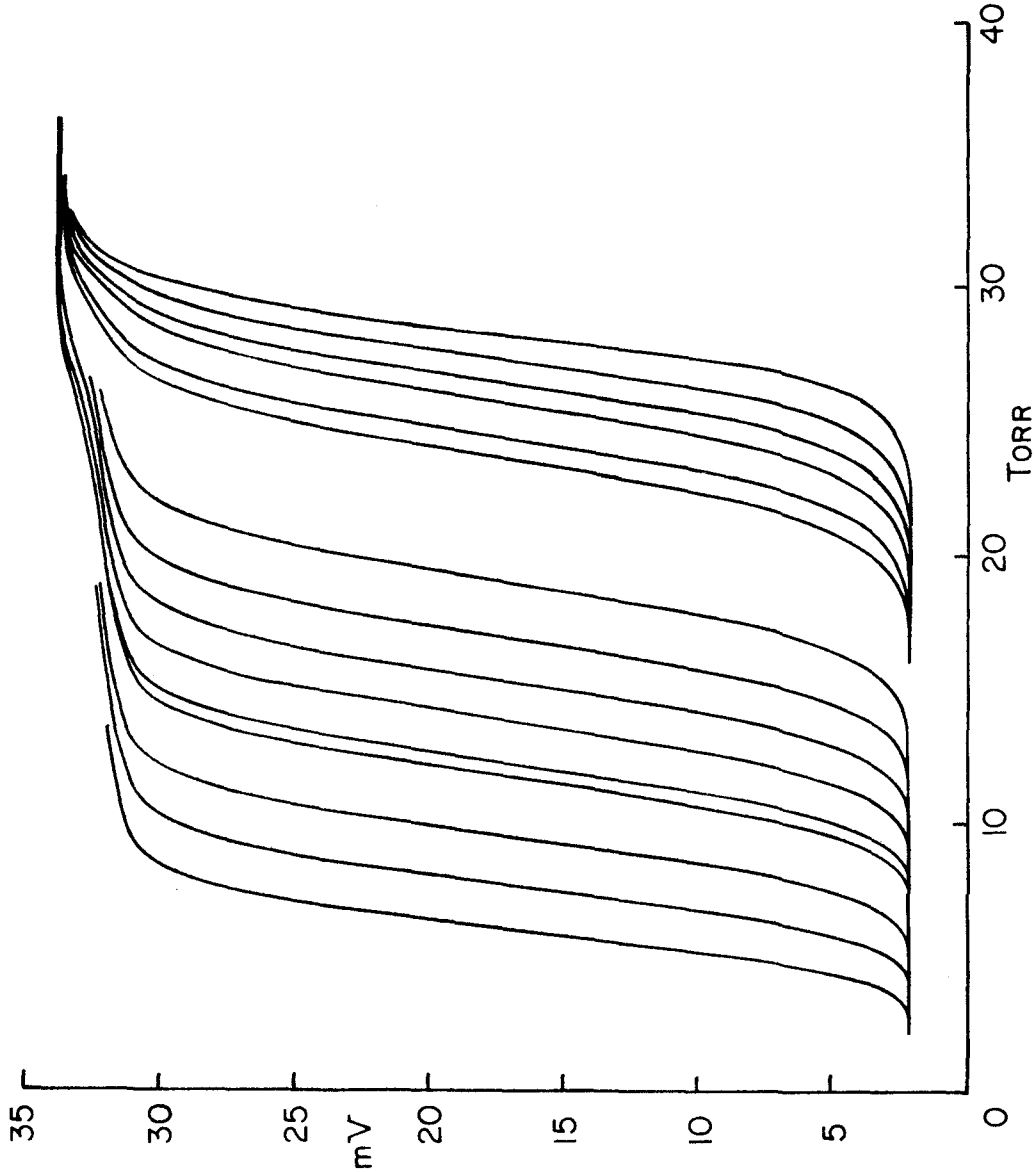

Figure III. 3. Typical family of superconducting detector transition curves. Magnetic field increases to the left. Bias current = 1 mA.

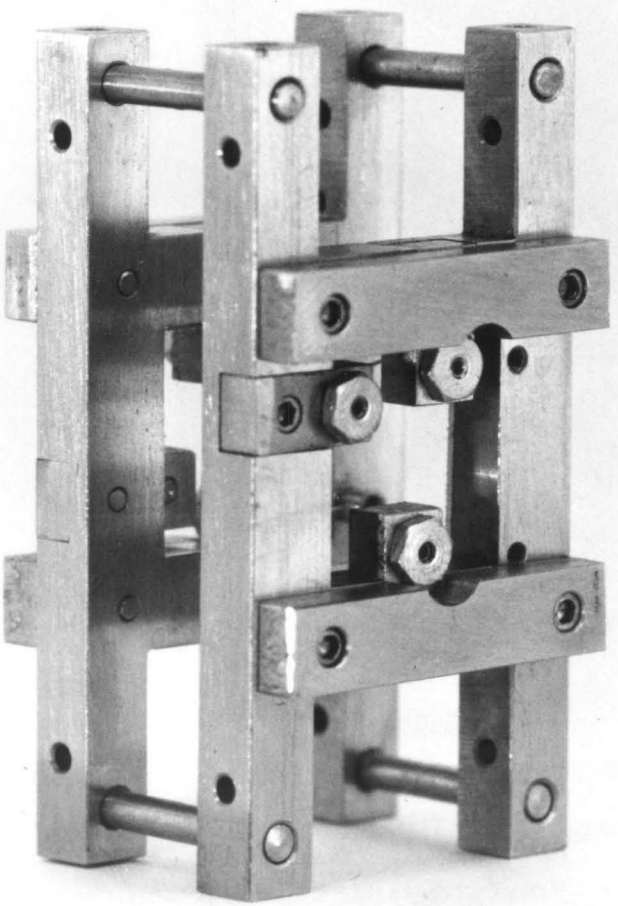

Figure III. 4. Second sound cell

provision for varying the emitter detector spacing from four millimeters to one centimeter. Alignment of the emitter and detector is by three set screws for each side arranged similar to a laser mirror mount. Tension is provided by stainless steel leaf springs which hold the emitter and detector against the alignment screws.

The magnet was fashioned by winding 40 A. W. G. copper magnet wire on a soft iron core. This is capable of providing fields at the detector of up to 200 gauss. The magnet yoke fits onto the detector mount in close proximity to the detector, but is easily demounted for alignment of the emitter and detector.

Alignment was accomplished at room temperature by means of a helium-neon laser and an optical setup. Because the entire structure is of the same material, there can be no differential contraction so alignment at room temperature is maintained at helium temperatures.

The optical path length from the laser to the cell was two meters. By bringing the reflected light from the surfaces of the emitter and detector back along the optical axis and into the dumping mirror of the laser (0.5 cm diameter) the maximum misalignment was 0.15 degrees which corresponds to an alignment of better than 0.1λ for second sound frequencies up to one megahertz.

The entire assembly of the jet, second sound cell, and supporting structure is shown in Figure III. 5. Figure III. 6 shows a top view schematic, drawn to scale, of the orifice, emitter, and detector.

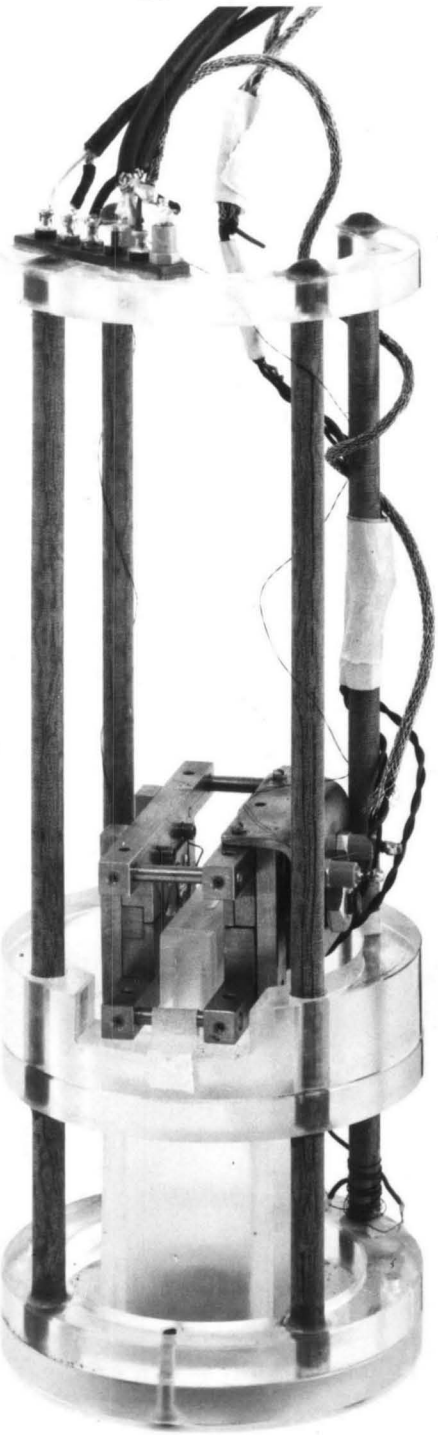

Figure III. 5. Support structure with jet

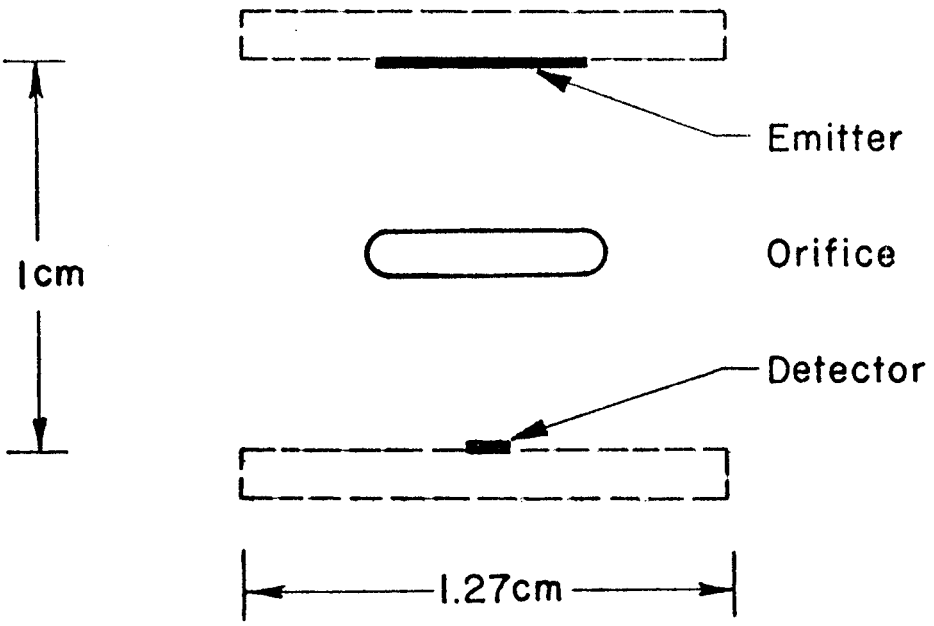

Figure III. 6. Top view schematic of the emitter, detector, and orifice geometry

III. C. Bath Temperature Regulation

Temperature regulation was accomplished by means of regulation of the bath pressure using a condom regulator. The pressure above the bath was monitored with a 100 mm full scale Barocell pressure transducer and converted to temperature using the 1958 He^4 temperature scale.

To maintain constant temperature for the duration of the experiment, it was necessary to maintain a constant heat input into the Dewar. This necessitated multiplexing between the jet heater and a ballast heater of approximately the same resistance wound around the base of the supporting structure. The efficiency of this system is shown in the graph of bath temperature vs. time for an experimental run (Figure III. 7). This graph represents a worst case of low temperature and high heat flux. It is worthwhile to note that at 1.6°K and comparable heat flux it would take a bath temperature change of approximately thirty millidegrees to produce a change in bulk attenuation at 100 kHz equal to 10% of the Gorter-Mellink attenuation. Therefore, the limitation imposed by bath temperature regulation is 0.1% of the Gorter-Mellink attenuation.

The current for the two heaters was supplied by a Hewlett-Packard Model 6299A Harrison DC power supply, and was monitored by measuring the voltage drop across a 100 ohm resistor in series with the heaters. This voltage was fed into one channel of an analog channel selector (see Ref. 1, Appendix 1 for details). The DC output from the Barocell formed a second channel. The analog channel selector multiplexed the two voltages into the guarded

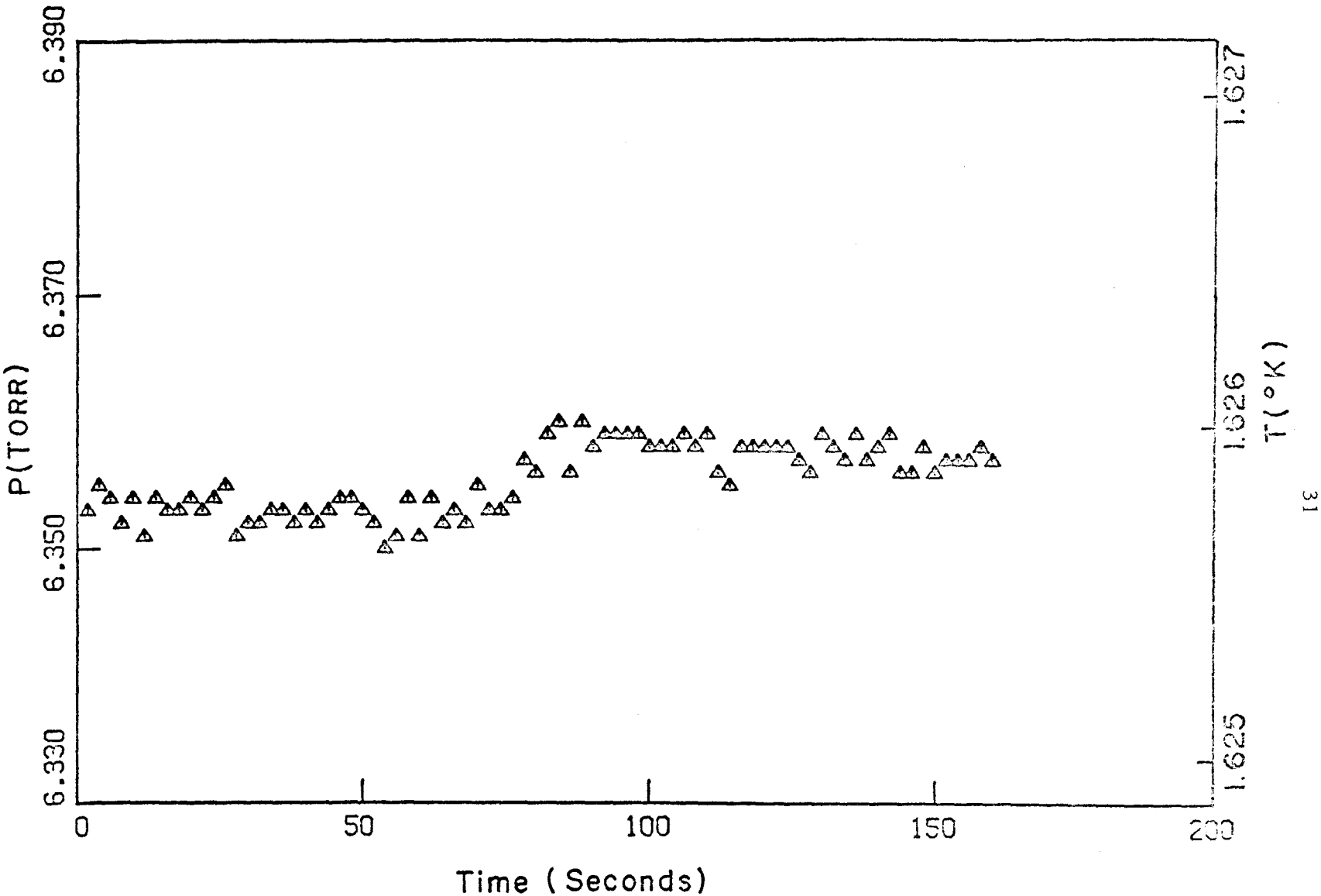

Figure III. 7. Bath temperature during an experiment for a heat flux of 2.88 Watts/cm^2.

input of a Hewlett-Packard 3450A multifunction meter with 6 digit resolution. This digitized the two voltages and printed them at one second intervals on a Hewlett-Packard 5050B printer, providing a record of the bath temperature and heater current during the run. Alternatively, the digital output from the voltmeter could be formatted into four 8-bit words and written onto magnetic tape using a Kennedy incremental tape recorder. This was used also to record the second sound detector voltage-temperature characteristics. A block diagram of the pressure sensor and heater electronics is shown in Figure III. 8.

III. D. Electronics

A block diagram of the electronics for the generation and detection of second sound is shown in Figure III. 9. It is easiest to discuss the emitter and detector electronics separately. The two systems are, in fact, integrally coupled through the wave analyzer's frequency output.

III. D. 1 Emitter Electronics

The heart of the emitter system is a General Radio 1310B sine wave generator with a frequency range of 2 Hz to 2 MHz and a short term drift of 0.3 p.p.m. over 10 minutes. This oscillator is capable of being synchronized to an external reference signal which was derived from the wave analyzer's beat frequency oscillator (B. F. O.) output. The B. F. O. signal was converted to a square wave and its frequency digitally divided in half in a device

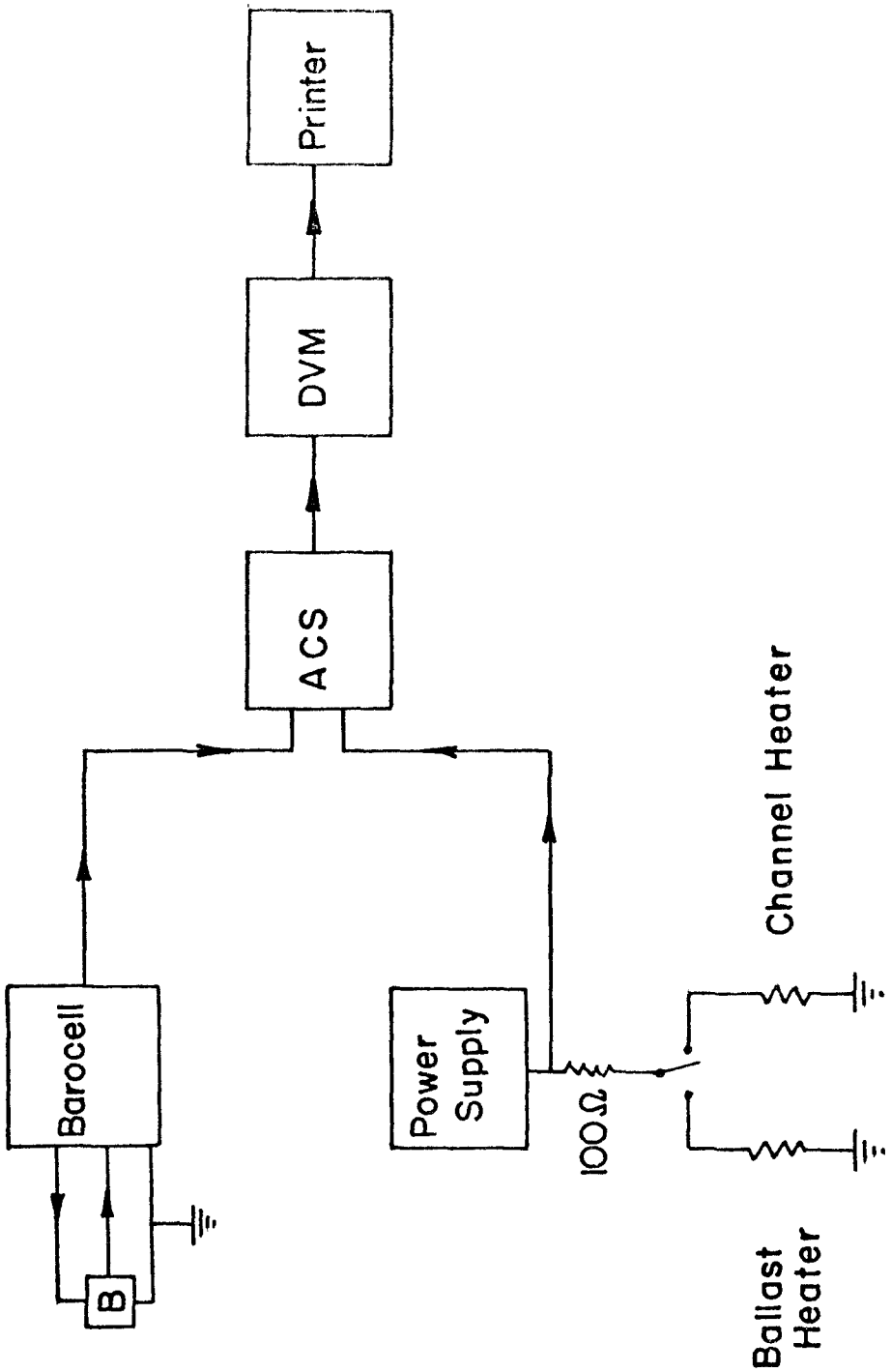

Figure III. 8. Block diagram of the heater and bath temperature regulation electronics. ACS is the analog channel selector which selectively switches input to the digital voltmeter.

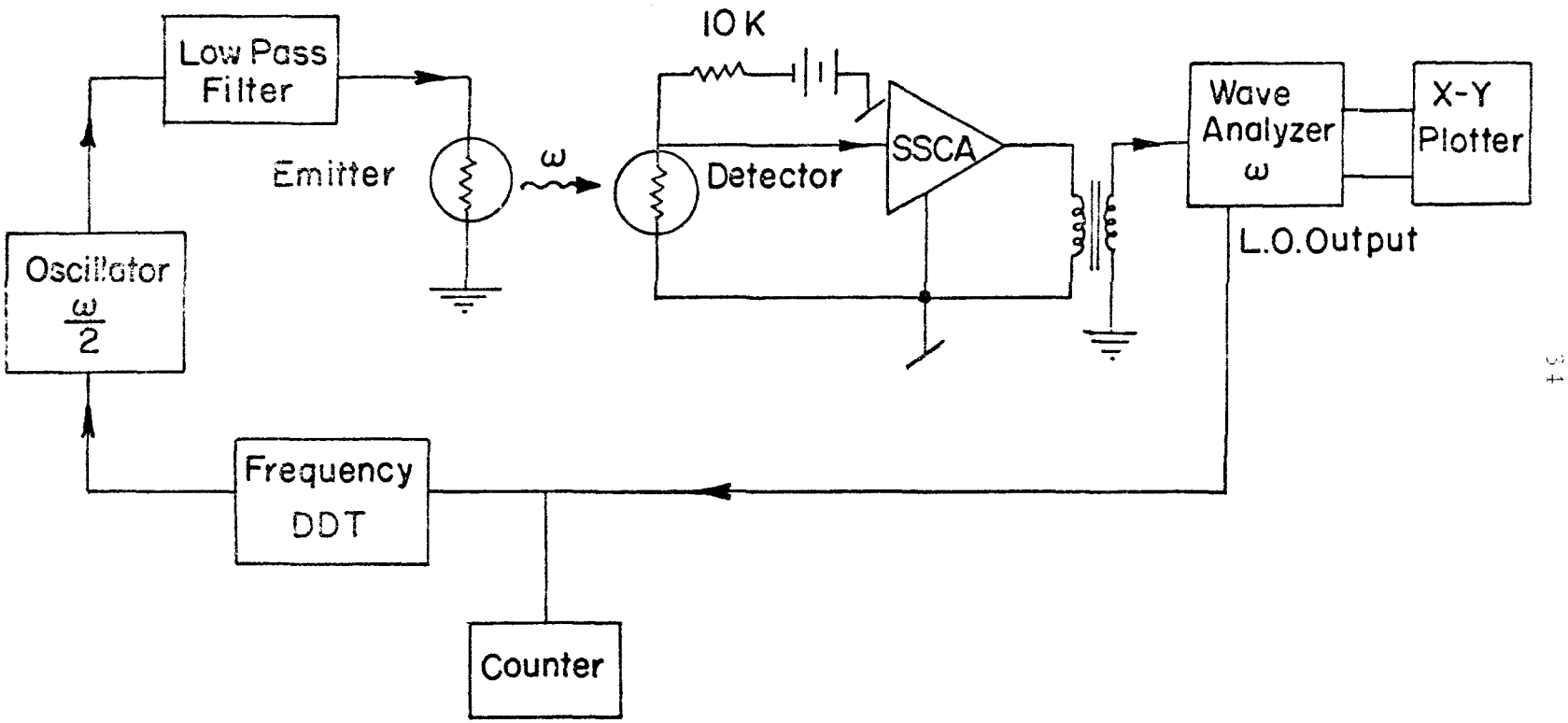

Figure III. 9. Second sound electronic instrumentation. DDT is a digital frequency divider. SSCA stands for small signal current amplifier.

labeled "Frequency DDT". This synchronized the oscillator to exactly half the center frequency of the wave analyzer's passband and also enabled the scanning local oscillator of the wave analyzer to sweep the second sound frequency. This method of frequency division is digitally precise as compared to the usual frequency doubling by a nonlinear element which has a typical accuracy of about one percent.

The other parts of the emitter circuit are a counter and filter. The counter was a General Radio Model 1192 B which gave the second sound frequency accurate to 0.001 kHz, and the filter was an Ithaco Model 4213, operated as a low pass filter whose corner frequency was set just above the maximum oscillator frequency. This reduced second harmonic generation in the emitter circuit, and its 50 ohm output impedance matched to the cables and emitter impedance. Particular care had to be taken to avoid any second harmonic generation because electromagnetic radiation of the second harmonic of the oscillator frequency would appear to the detector the same as second sound.

III. D. 2 Detector Electronics

The detector electronics consisted of a small signal current amplifier (SSCA) and wave analyzer. The amplifier had a bandwidth of 30 MHz with a noise figure of 3.3 nanovolts/$\sqrt{\text{Hz}}$, and served as a preamplifier. It was originally built as a current amplifier for a photomultiplier tube but since its 2200 ohm input impedance was large compared to the detector resistance it served

equally well as a voltage amplifier. With detector efficiencies as high as 0.6 volts/^{o}K this current amplifier gives a signal to noise ratio of unity for 50 nanodegree second sound amplitudes. Minor changes in the electronics would improve this by a factor of 10 but amplifier noise did not represent a limitation in this measurement. The SSCA and the detector formed the low level part of the signal detection system and so were provided with a separate ground.

The two wave analyzers used were a Hewlett-Packard Model 3590A with 3594A sweeping local oscillator for frequencies below 600 kHz and a Hewlett-Packard Model 310A with 297A sweep drive for frequencies up to 1.2 MHz. These provided narrow band filters and also the reference signal used to sweep the second sound cavity through its resonance. Both analyzers provided a DC ramp proportional to the center frequency of the filter and a DC voltage proportional to the RMS value of the signal component within the passband. The two outputs from the wave analyzer were fed into an X-Y Plotter (Hewlett Packard 7004 B). Thus the wave analyzer generated a plot of second sound amplitude versus frequency; i.e., the second sound spectrum of the resonant cavity.

REFERENCES

1. Paul E. Dimotakis, Ph. D. Thesis, California Institute of Technology (1972).

IV. METHOD OF MEASUREMENT AND PRELIMINARY EXPERIMENTS

IV.A. Second Sound Resonance Technique

A traveling second sound wave in the x direction can be represented as

$$e^{-\alpha x} \; e^{i\omega(t - x/u_2)} \quad .$$

The second sound resonator is ideally formed by an infinite plane emitter with the detector being an infinite perfect reflector having a small sensing element in its center. The geometrical optics approximation is valid here provided the second sound wave length is much smaller than the emitter dimensions. Notarys (Ref. 1) found that his detectors exhibited negligible reflective loss even at very high frequencies. If the power input per unit area to the emitter is $Q/A \cos\omega t$, then the amplitude at the detector will be

$$(\Delta T)_{ss} = \frac{Q}{A} \frac{1}{\rho c u_2} \frac{1}{\left(\cosh^2 \alpha D - \cos^2 \frac{\omega D}{u_2}\right)^{\frac{1}{2}}} \cos\left\{\omega t - \varphi\right\}$$

$$\varphi = \tan^{-1}\left(\coth \alpha D \tan \frac{\omega D}{u_2}\right) \quad .$$

In this formula c is the heat capacity and D is the spacing between the emitter and detector.

A resonance condition is satisfied whenever

$$\frac{\omega D}{u_2} = n\pi \quad .$$

At a fixed temperature this can be accomplished by varying ω, however it can also be accomplished by holding the frequency fixed and allowing the bath temperature to drift, thus changing u_2. The speed of second sound can therefore be measured at a fixed temperature by measuring the frequencies of two successive resonances, i.e.,

$$u_2 = (\omega_{n+1} - \omega_n) \frac{D}{\pi} \quad . \tag{2}$$

An expression for the attenuation can be derived from Eq. 1 by the expansion of $\cosh^2 \alpha D$ for small argument and the expansion of $\cos^2 \omega D/u_2$ near a resonance. By measuring the width, $\Delta\omega$, of the resonance curve at $1/\sqrt{2}$ of the maximum height one finds for a frequency resonance

$$\alpha = \frac{\Delta\omega}{2u_2} \qquad \text{(T constant)} \quad . \tag{3}$$

For a temperature resonance the expansions give

$$\alpha = \frac{\Delta T}{2} \frac{\omega^2}{u_2^2} \frac{du_2}{dT} \qquad (\omega \text{ constant}) \quad . \tag{4}$$

If there is an additional attenuation, $\Delta\alpha$, when the jet is turned on, then α in the above formulas is replaced by $\alpha + \Delta\alpha$. There is an easier way to get $\Delta\alpha$ provided α has already been measured. One can find $\Delta\alpha$ by a comparison of the height of the resonance peaks for the jet on and jet off, i.e.,

$$\frac{(\Delta T_{ss})_{on}}{(\Delta T_{ss})_{off}} = \left\{ \frac{\cosh^2 \alpha D - 1}{\cosh^2 (\alpha + \Delta\alpha) D - 1} \right\}^{\frac{1}{2}} \quad .$$

Expansion of the cosh terms gives

$$\Delta\alpha = \alpha \left\{ \frac{(\Delta T_{ss})_{off}}{(\Delta T_{ss})_{on}} - 1 \right\} \qquad (5)$$

IV. B. Initial Checkout Experiments

Several experiments were performed in order to test the limitations and reliability of the second sound apparatus and to allay some of the fears of the experimenter about competing effects. These experiments will be described in this section.

IV. B. 1 Second Sound Experiments

Three experiments were performed to test the second sound apparatus. The first was a simple experiment designed to demonstrate that second sound was, in fact, being measured and not electromagnetic or inductive heating of the detector which was an anticipated problem. Provision was made for the insertion of a small shutter between the emitter and detector. Because the wavelength of light at 1 MHz is approximately 300 meters the shutter blocks second sound but does not affect the electromagnetic radiation. The results at a frequency of 1 MHz are shown in Figure IV. 1. This clearly shows the resonance pattern and also the limitations imposed by electromagnetic pickup. Similar spectra were also measured at 100, 300 and 500 kHz.

Another quicker method of determining the relative amplitude of second sound and radiation is to measure the amplitude of the received signal versus the input signal. Second sound increases as

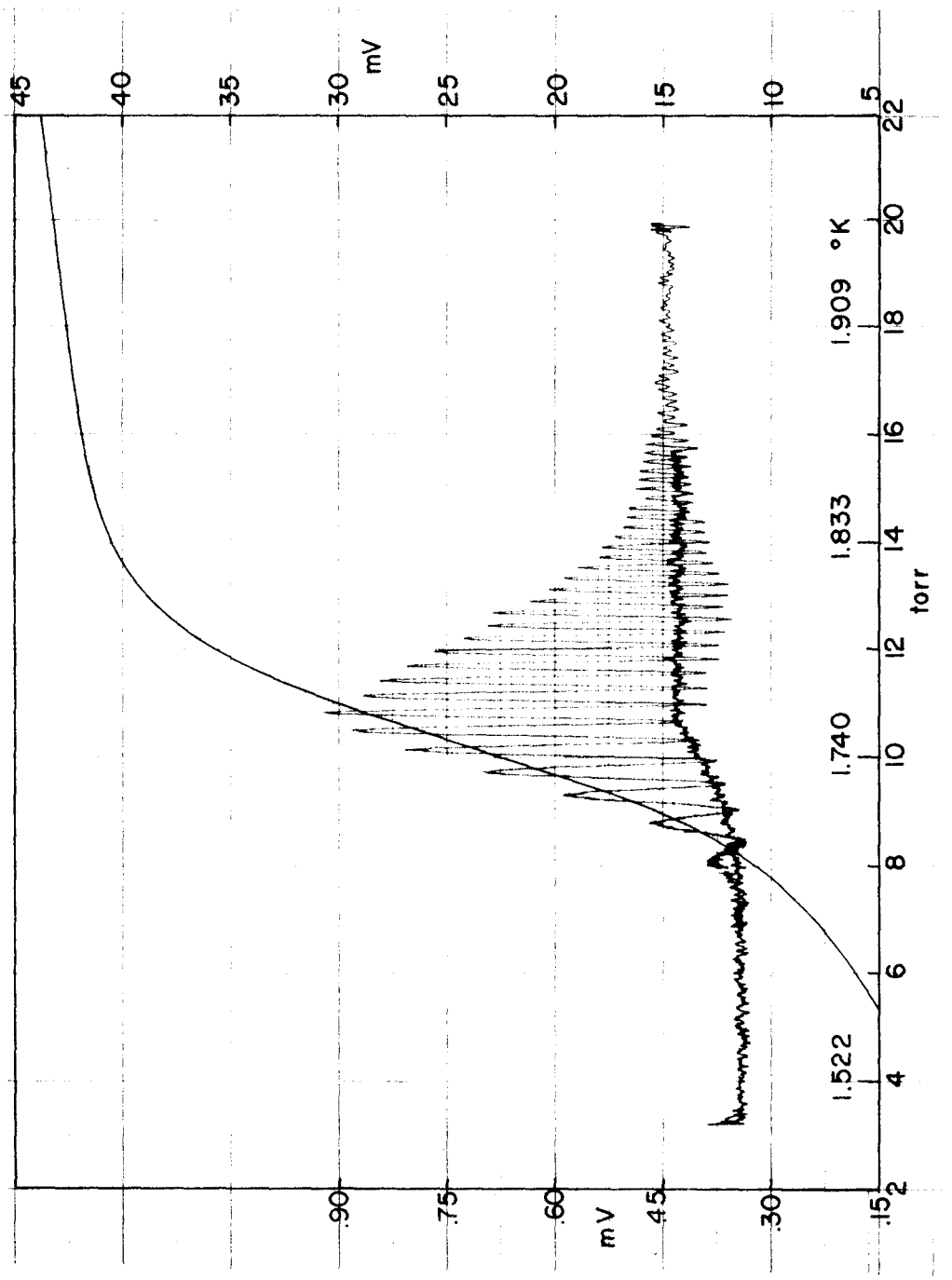

Figure IV.1. A temperature resonance curve at 1 MHz. The signal is a convolution with the slope of the detector characteristic also shown. Right vertical scale is for the detector; left scale is for the signal.

the input voltage squared while radiation increases linearly with voltage input. After the installation of the emitter circuit filter and crossed current geometry, which significantly reduced radiative effects, the noise due to radiation was insignificant compared to bath temperature drift which was the major limitation.

The second check on the second sound apparatus concerned diffraction of the second sound beam. If the second sound beam spread due to diffraction, this would look like an additional attenuation although it should not change the attenuation due to the jet. The volume attenuation of second sound was measured versus temperature at several frequencies. The results at 250 kHz are plotted in Figure IV. 2. For comparison Hanson and Pellam's (Ref. 2) data are also plotted. One can conclude that at 250 kHz diffraction is a negligible loss. However, it was found that at 100 kHz there is a spreading of the beam due to diffraction. A simple optics argument establishes that at 100 kHz the spreading angle is 2. 3 degrees while at 250 kHz it is only 0. 8 degrees. An additional check is the measurement of the speed of second sound shown in Figure IV. 3. The error bars represent the unavoidable uncertainty in the emitter-detector spacing. It can be seen that a uniform translation of all the points by a small distance would bring this data into essentially perfect agreement with the results of earlier experimenters (data taken from Ahlers, Ref. 3).

IV. B. 2 Temperature Gradient Measurements

The counterflow jet used in the investigation of Dimotakis

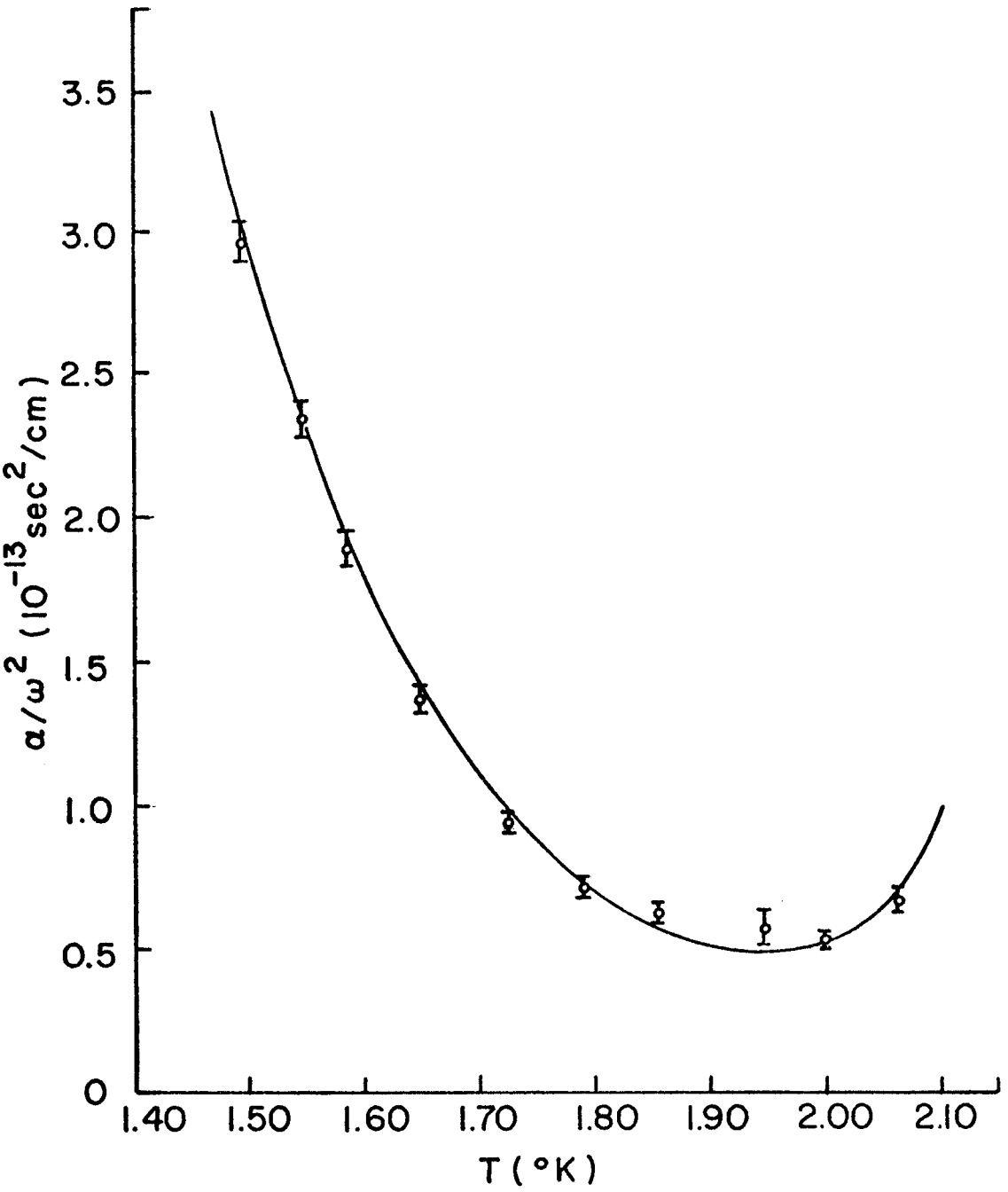

Figure IV. 2. Bulk attenuation of second sound vs. T. Frequency was 250 kHz. Solid line is an interpolation of Hanson and Pellam's data (Ref. 2).

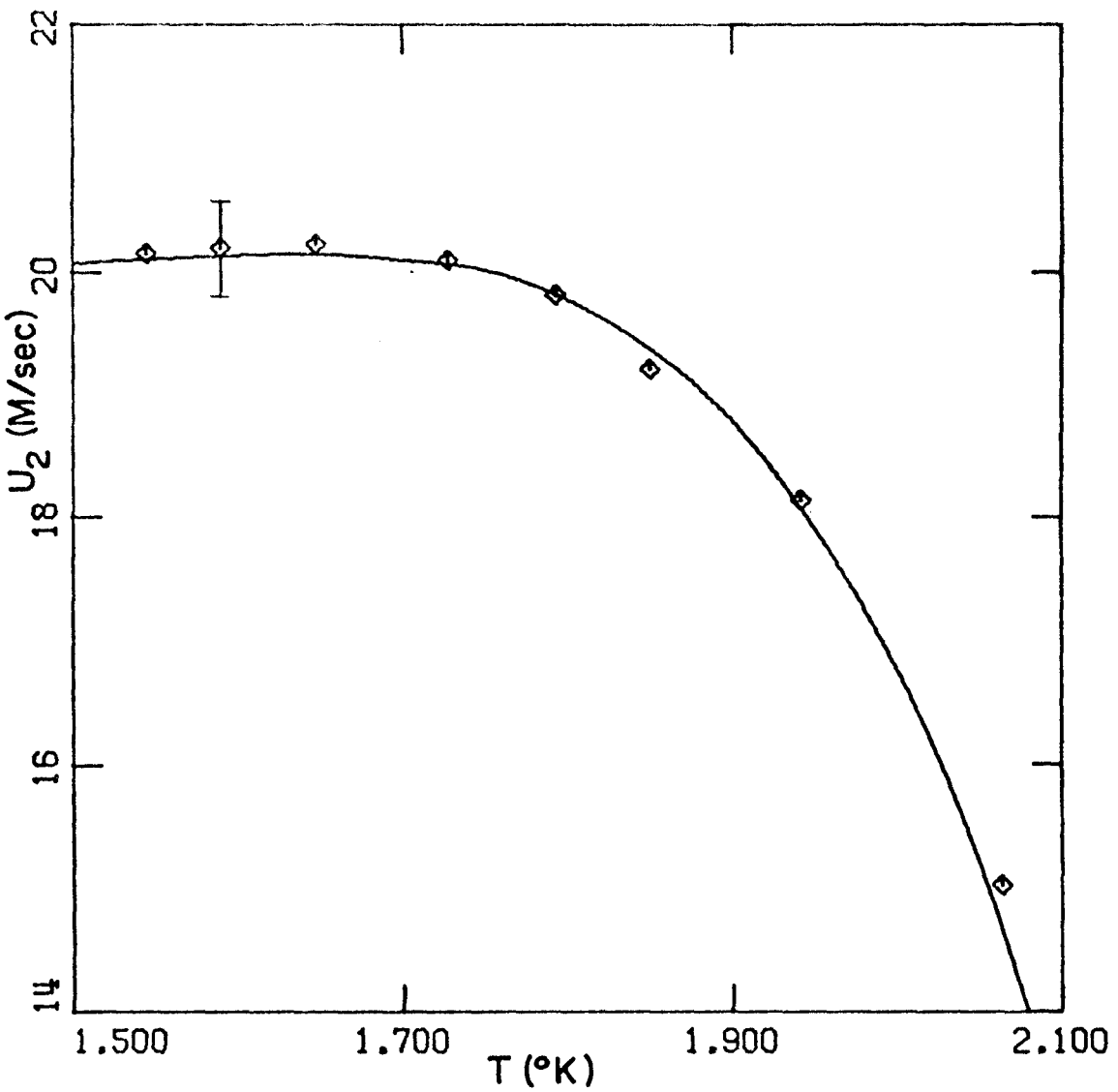

Figure IV. 3. Second sound speed vs. T. Solid line is an interpolation of Greywall and Ahlers data (Ref. 3).

and Broadwell (Ref. 4) had an axisymmetric shape while the jet used in the present experiment was somewhat more two-dimensional. Therefore, it was necessary to establish the behavior of the temperature gradient along the center line of the two-dimensional jet. To do this a small carbon thermometer (a cube approximately 0.01 inches on each side) was traversed along the jet center line. The method of measurement was essentially the same as that used by Dimotakis and Broadwell.

A typical traverse is shown in Figure IV.4. The distinctive feature once again is that the temperature gradient takes place almost entirely within the straight section of the jet close to the orifice and disappears within one jet width of the orifice.

For a further comparison the measured temperature gradient in the straight section was fitted to the equation $\nabla T = b(T)\, q^3$ which describes the gradient due to mutual friction in a channel. The measured values of $b(T)$ are plotted in Figure IV.5 along with several points from the measurements of Broadwell and Liepmann (Ref. 5) in the convergent-divergent nozzle geometry and Model I data of Dimotakis and Broadwell (Ref. 4). The solid line is computed from the theoretical equation

$$b(T) = \frac{A(T)\rho_n}{s(\rho_s sT)^3} \quad .$$

$A(T)$ is the coefficient of mutual friction in Equation II.11 which is given by the equation

$$\log_{10} A(T) = 1.10 + 3.12 \log_{10} T + [0.0076/(1 - T/T_\lambda)]$$

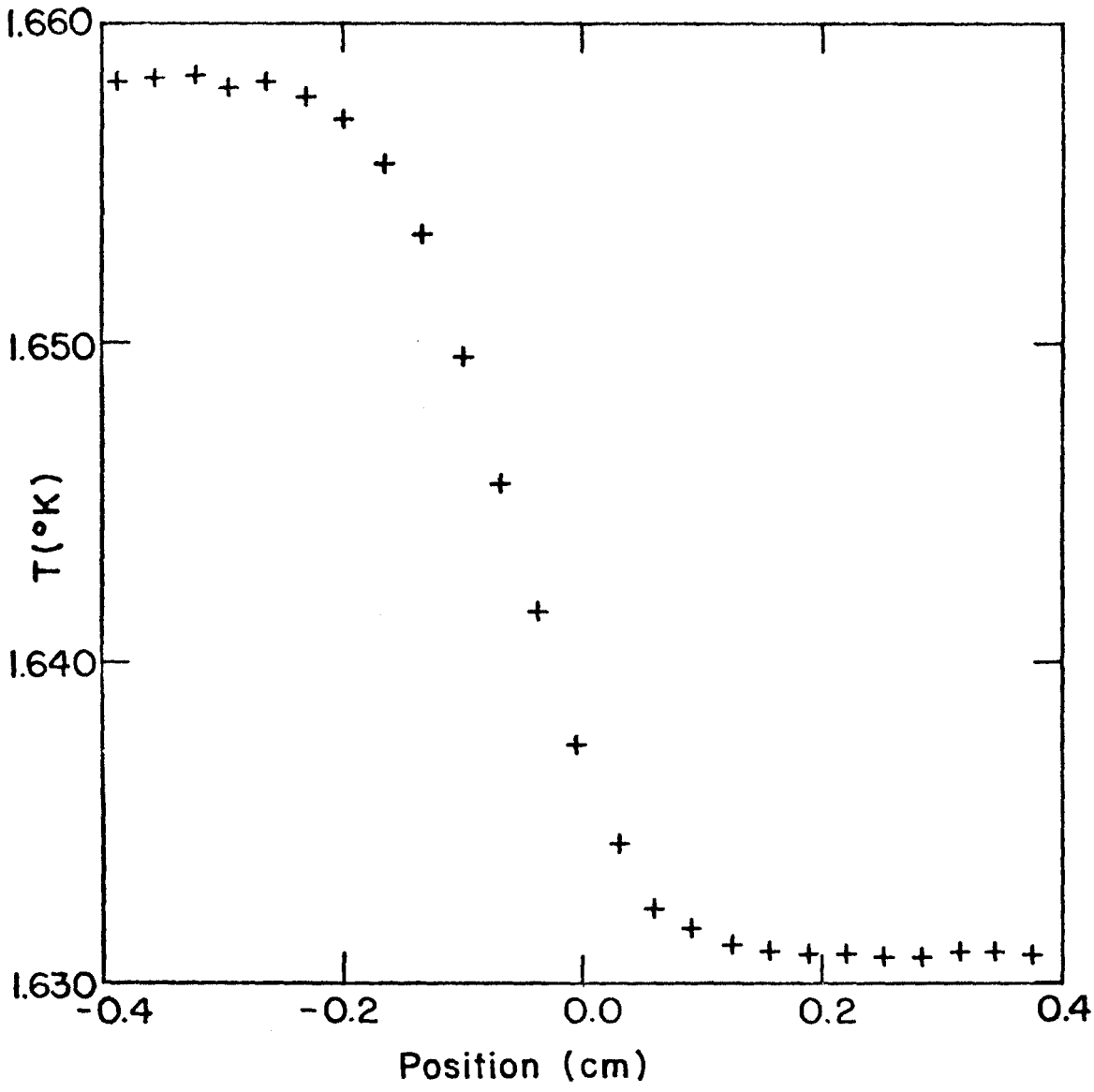

Figure IV. 4. Temperature gradient measured in the jet. The exit plane is at 0.0 and positive positions are in the free jet. Heat flux = 3.46 Watts/cm^2.

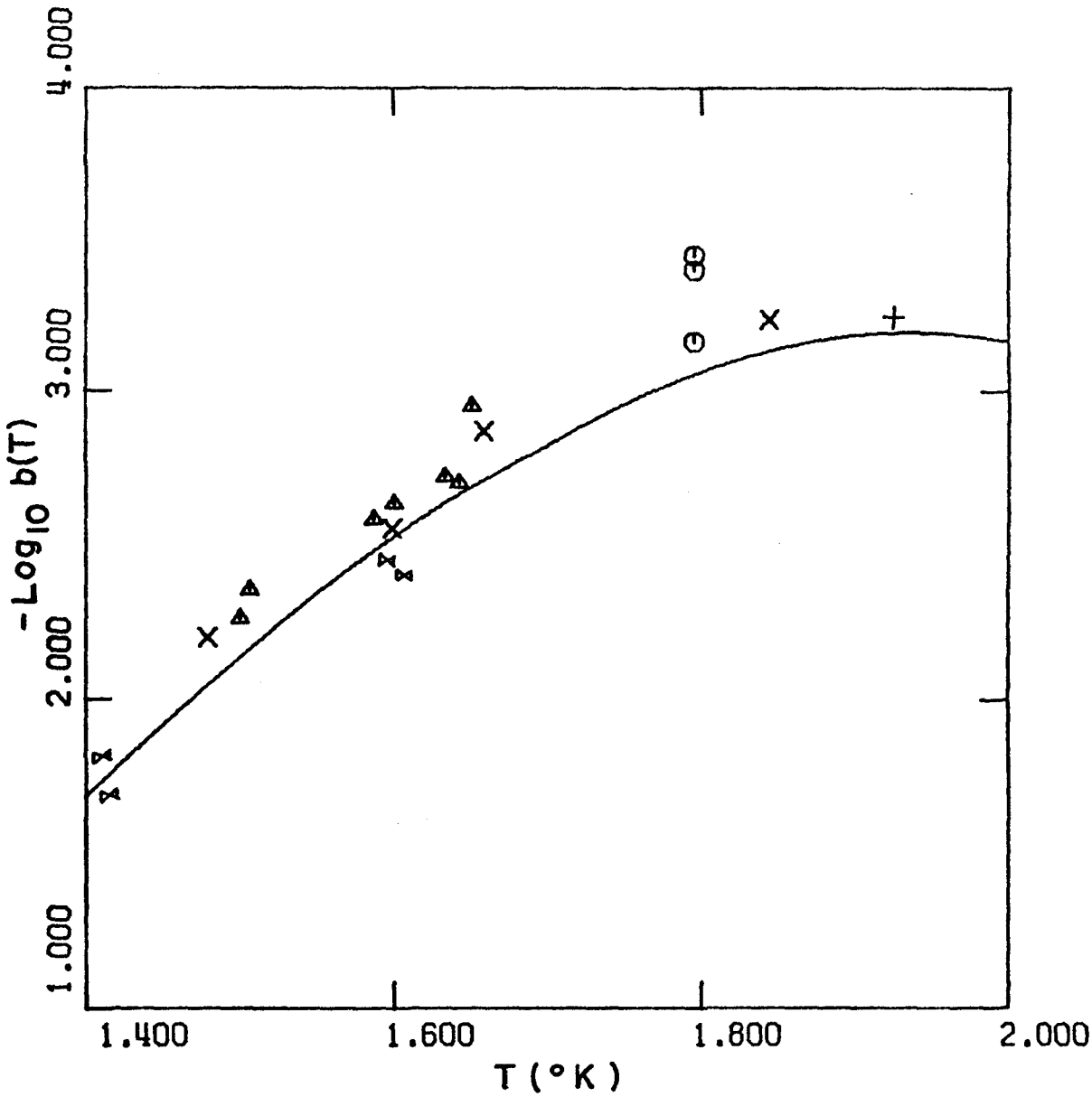

Figure IV. 5. Gradient coefficient from the measurements in the straight nozzle section. X's are measurements of Ref. 4 and Ref. 5.

based on the Model II data of Dimotakis and Broadwell. Their Model II had a long straight section for more accurate gradient measurements. The data shown in Figure IV.5, therefore, demonstrates the consistency of the gradient measurements on the two-dimensional jet with those of the axisymmetric jet, and also the accuracy of the Gorter-Mellink law in a channel.

REFERENCES

1. H.A. Notarys, Ph.D. Thesis, California Institute of Technology (1964).
2. W.B. Hanson and J.R. Pellam, Phys. Rev. 95, 321 (1954).
3. D.S. Greywall and G. Ahlers, Phys. Rev. 7, 2145 (1973).
4. P.E. Dimotakis and J.E. Broadwell, Phys. Fluids 16, 1787 (1973).
5. J.E. Broadwell and H.W. Liepmann, Phys. Fluids 12, 1533 (1969).

V. ATTENUATION MEASUREMENTS

V. A. Data-Taking Procedure

This section is an outline of the basic experimental run procedure for measuring the added attenuation of second sound due to the counterflow jet. The emitter detector spacing and distance from the orifice were fixed while the apparatus was at room temperature before a set of experimental runs.

At liquid helium temperatures the run was started by setting the bath temperature using the condom regulator. The detector was then biased in the middle of its transition at that temperature by means of a ten-turn potentiometer on the magnet current supply. A resonance peak was found by scanning the wave analyzer close to the desired operating frequency. Then the amplitude of the General Radio oscillator was adjusted so that the noise level was less than one percent of the second sound amplitude on resonance. This could always be accomplished with a power input less than 0.01 Watts/cm^2 into the emitter and it was experimentally verified that this caused no finite amplitude effects or power broadening of the resonance.

Finally the heat flux of the jet was set by adjusting the current into the ballast heater. The bath was allowed to reach its new equilibrium pressure, usually within a few millitorr of the initial pressure and not enough to cause a change in the detector bias point. A frequency sweep was then made with the jet off. At the end of this sweep the sweeping local oscillator of the wave

analyzer was returned to its starting point and the jet turned on. Although it took less than two seconds for the jet to turn on, thirty seconds usually elapsed between the off and on sweeps allowing the bath to come fully to equilibrium once again. A series of such runs was made at each temperature with heat fluxes increasing from 0.3 Watts/cm^2 until it was no longer possible to maintain constant bath temperature. This occurred at heat fluxes between 2.5 Watts/cm^2 at lower temperatures and 4 Watts/cm^2 at the highest temperatures measured.

V. B. Discussion of the Experimental Resonance Curve

A typical experimental run at $T = 2.056^{\circ}K$ is shown in Figure V.1. The higher trace was with the jet off and the lower trace with the jet on. For this run the resonant frequency was approximately 100.74 kHz and the heat flux at the orifice was 1.23 Watts/cm^2. The additional attenuation is quite noticeable.

There is a slight shift in frequency of about 10 Hz between the peaks with the jet on and the jet off. This was almost always present but not consistent in either size or direction, although the shift was never more than 30 Hz. Sometimes the peak with the jet on was shifted to a higher frequency. Several effects could change the index of refraction for second sound, but none of these would give a change in resonant frequency of more than one Hertz. It was also noticed that if a measurement was repeated twice with the jet off both times there was still a small frequency shift. One can only conclude that the major portion of this frequency shift is

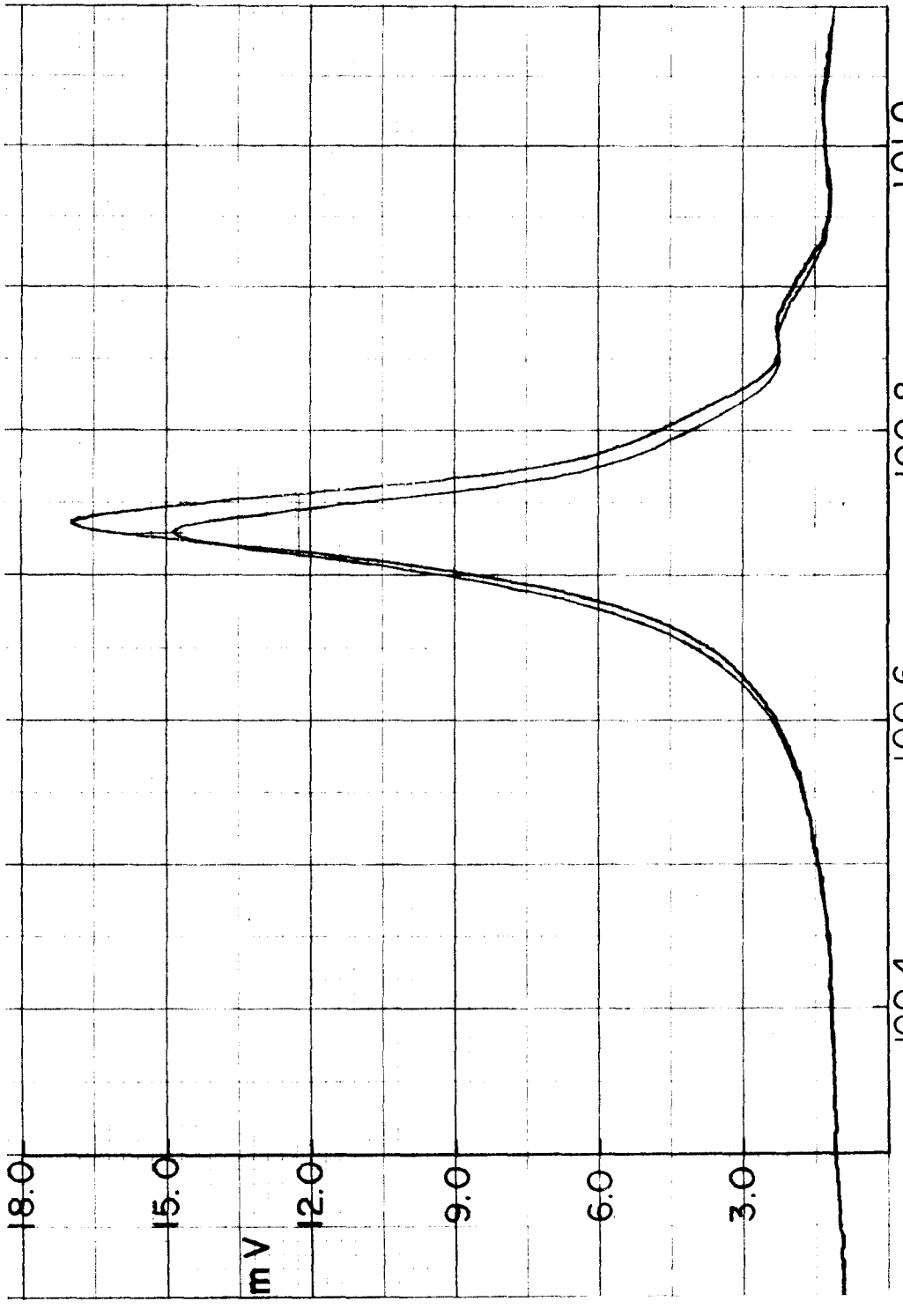

Figure V.1. Frequency resonance at T = 4.062K and heat flux of 1.23 Watts/cm^2. Upper trace is with the jet off and lower trace is with the jet on.

due to the short term drift of the wave analyzer sweep oscillator. Note that one is asking for unreasonable stability from an analog instrument. With a better frequency source such as a digital synthesizer this effect could be examined further, however, the cost of such instrumentation precludes further investigation at this time.

Some justification is needed for measurements at frequencies as low as 100 kHz since non-negligible diffraction was observed at this frequency. Diffraction should not affect the relative attenuation measurements since the same loss of beam would be present both with the jet on and with the jet off. However, an experimental check was made just to be sure. The resonance curves were measured with the jet on and jet off at two frequencies, 100 kHz and 250 kHz. From these measurements the relative attenuation was computed in two ways. First, the total attenuation was computed for each peak using the width at .707 of the maximum in Eq. IV.3. Subtraction then gave the additional attenuation with the jet on. In addition, the change in attenuation was computed from the ratio of the resonant amplitudes and bulk attenuation using Eq. IV.5. The bulk attenuation at 250 kHz is the same as the attenuation measured with the jet off (see Figure IV.2). These four values of the additional attenuation were the same to within experimental accuracy, and this provides the justification for the 100 kHz measurements. It also shows that the additional attenuation due to the jet is independent of frequency.

When the second sound beam was close to the orifice, multiple peaks were observed where only one had been previously.

These coalesced into one peak at higher frequencies so the effect is probably due to reflections of the diffracted wave from the lucite structure. Therefore measurements at a distance downstream of 1/2 jet width were made only at frequencies above 250 kHz where diffraction was negligible.

V. C. Data Reduction

It was found that for a given temperature and position downstream of the orifice, the additional attenuation ($\Delta\alpha$) versus the heat flux (q) fell on a straight line when plotted on logarithmic graph paper; i. e.,

$$\log(\Delta\alpha) = \log I + n \log q \quad .$$

An example is shown in Figure V. 2. Therefore, one can consider all of the data in the form

$$\Delta\alpha = I q^{n}$$

where I represents the additional attenuation due to the jet at a heat flux of 1 Watt/cm^2.

The measured values of I for four positions are shown in Figures V. 3 to V. 6. In addition, a line which is computed from the best polynomial fit to the data is also plotted. Table V. 1 gives the measured value of the exponent, n .

For the 20 diameter measurements one straight line would not fit all the data on the log-log plot; however, the data at high heat fluxes and low heat fluxes could be fit separately by two straight lines of different slope and intercept. This possibly

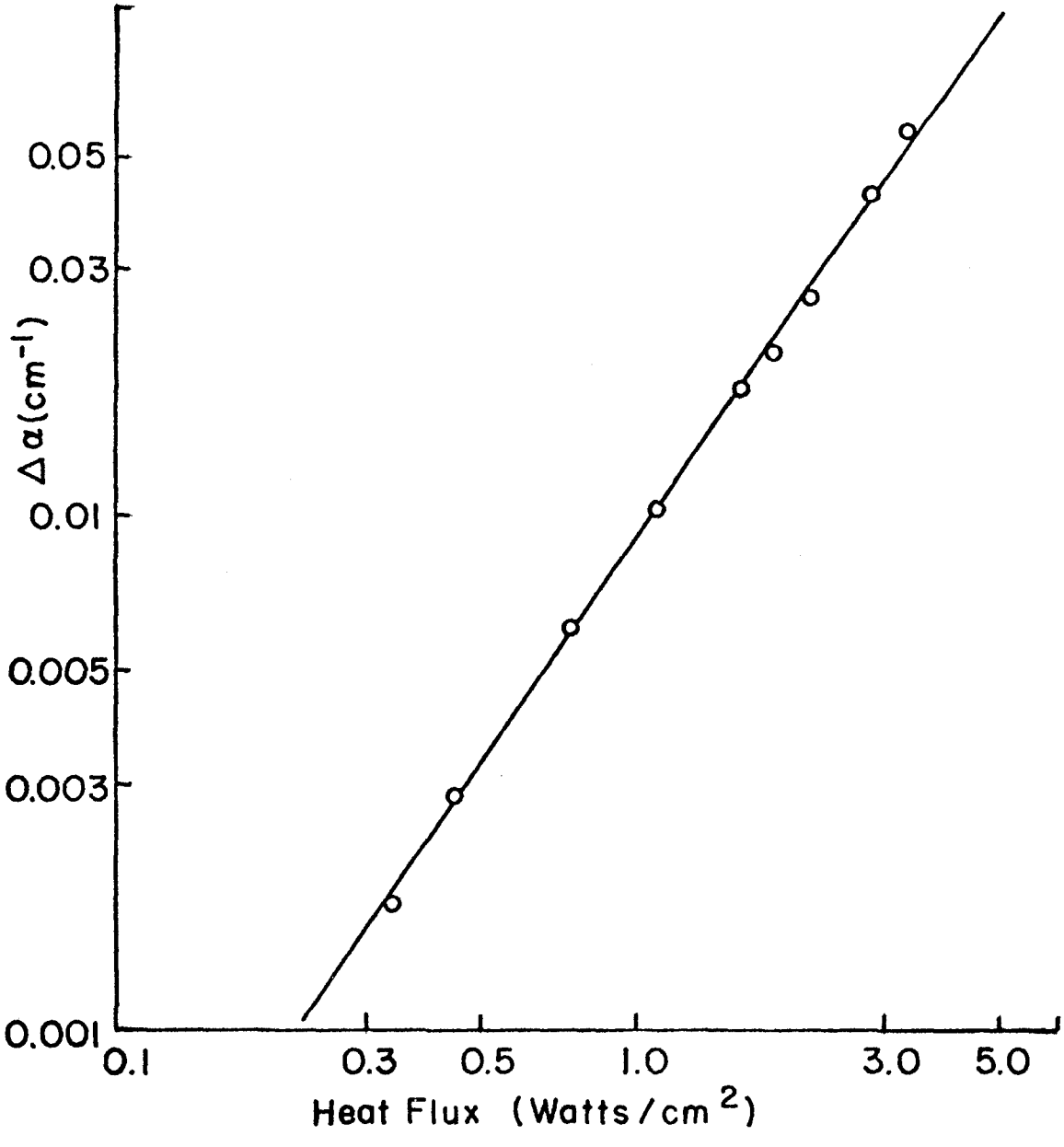

Figure V.2. Additional attenuation vs. heat flux at T = 1.623°K and 9.6 diameters downstream.

represents some type of transition between two flow regimes, a possibility that will be explored further in Section VI. Figure V.6 and the values in Table V.1 are for the line which fit the higher heat flux data.

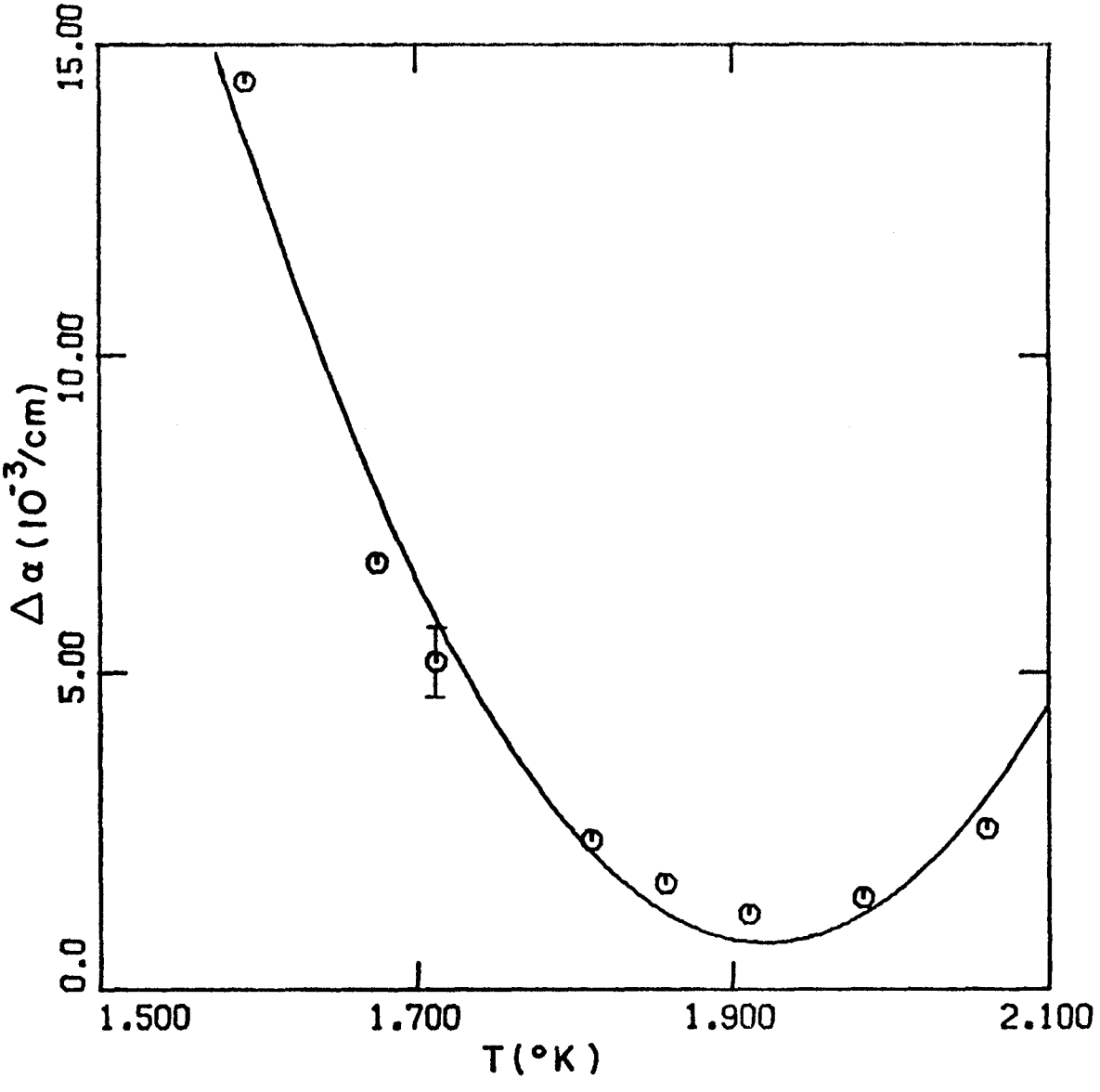

Figure V.3. Additional attenuation vs. T for a heat flux of 1 Watt/cm^2 at 3.2 diameters downstream.

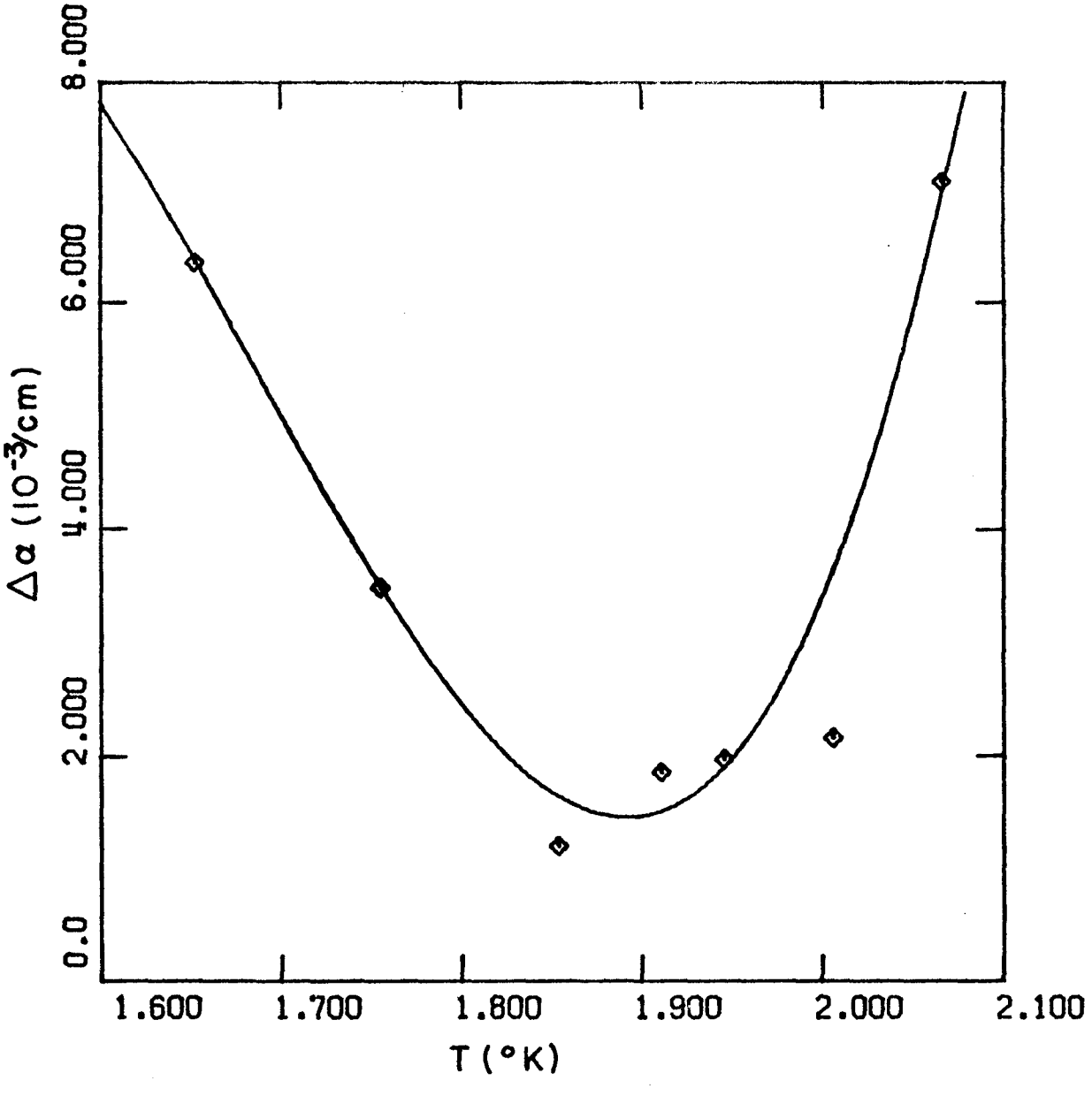

Figure V.4. Additional attenuation vs. T for a heat flux of 1 Watt/cm^2 at 1/2 diameter downstream.

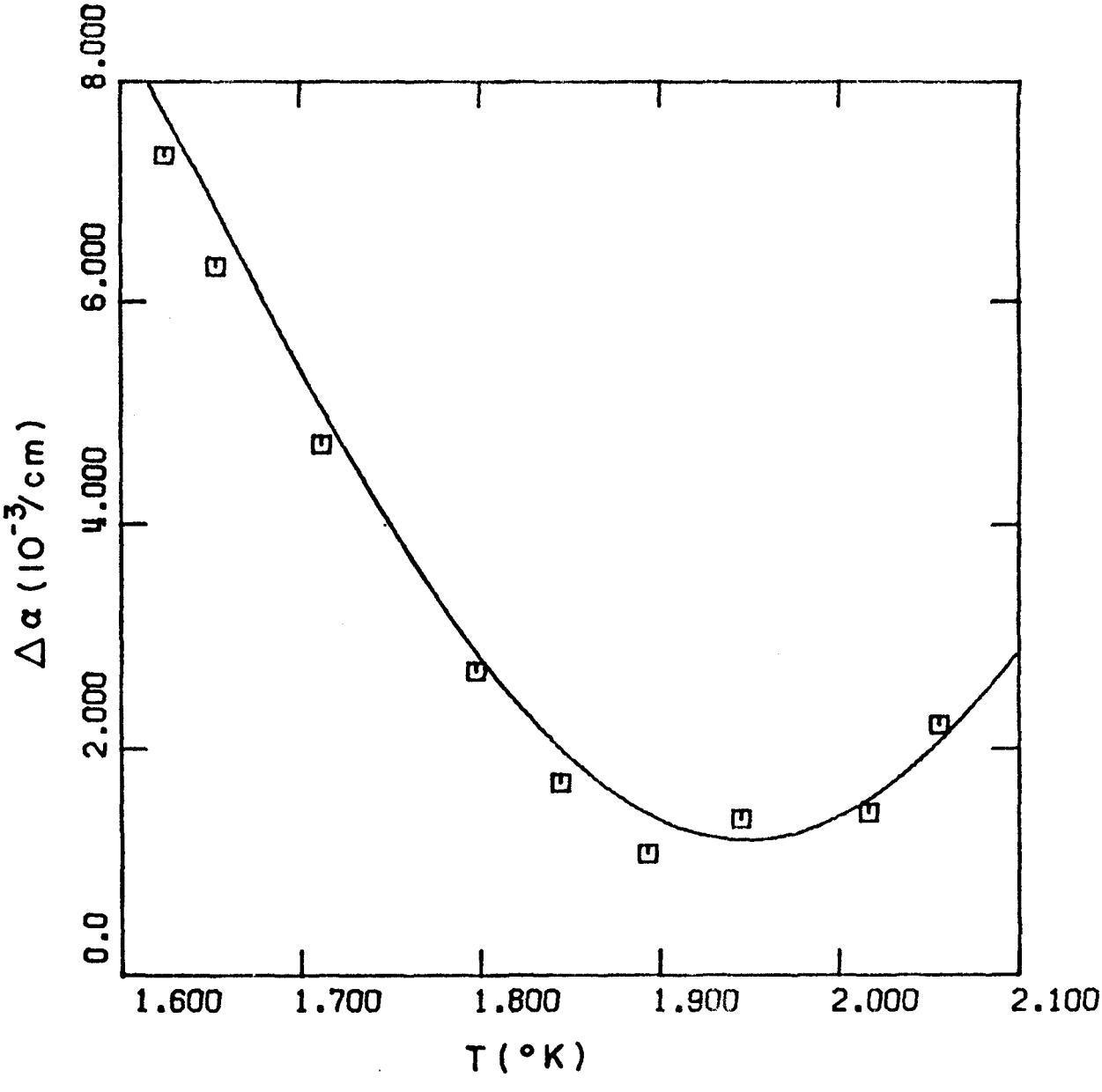

Figure V. 5. Additional attenuation vs. T for a heat flux of 1 Watt/cm^2 at 9.6 diameters downstream.

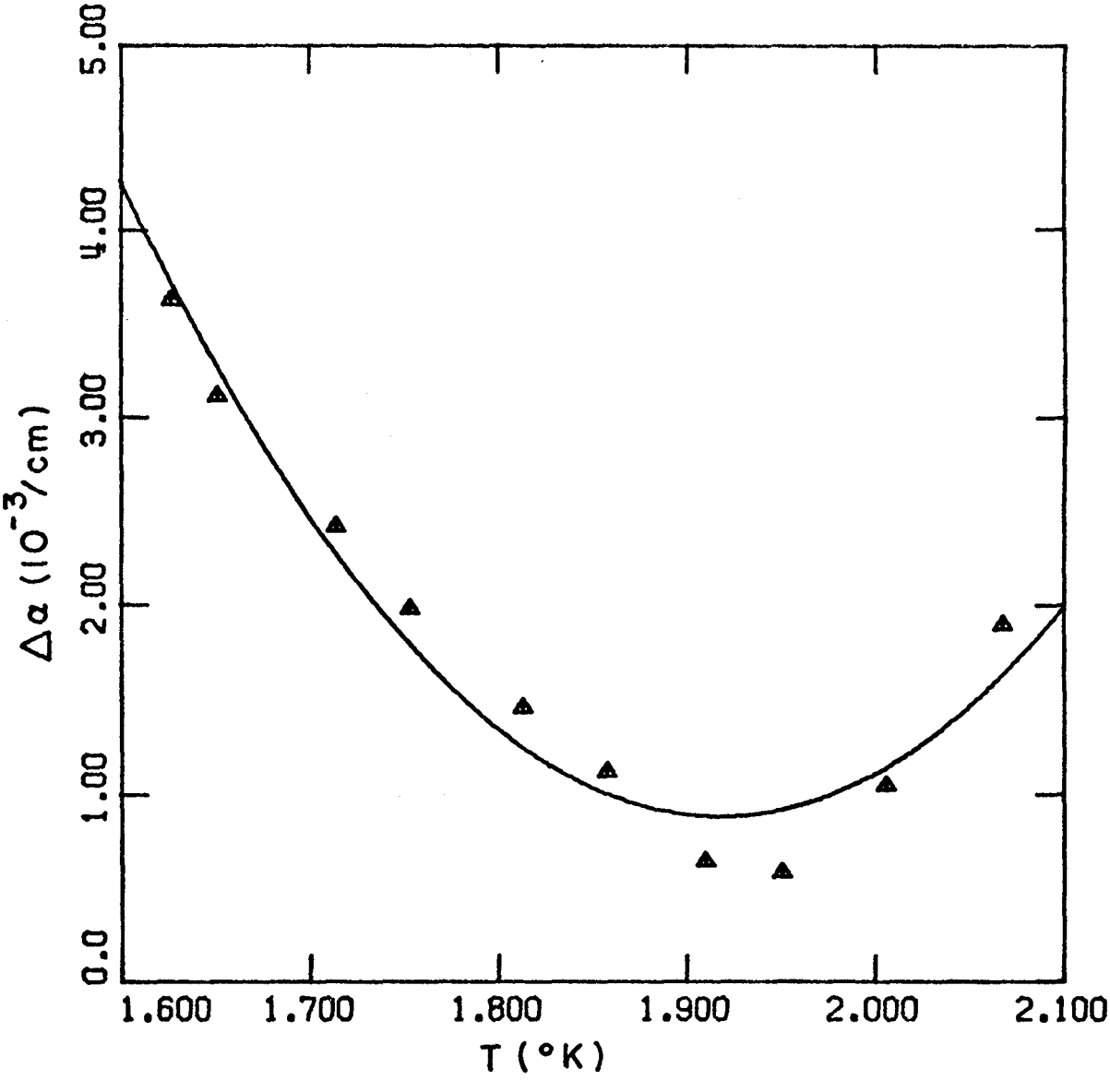

Figure V. 6. Additional attenuation vs. T for a heat flux of 1 Watt/cm^2 at 20 diameters downstream.

Table V.1. - OBSERVED POWER DEPENDENCE

x/d = 0.5		x/d = 3.2		x/d = 9.6		x/d = 20	
T	n	T	n	T	n	T	n
1.652	2.39	1.593	1.43	1.625	1.47	1.627	1.25
1.755	2.23	1.676	1.69	1.653	1.56	1.651	1.47
1.854	2.59	1.713	1.64	1.712	1.61	1.714	1.30
1.911	2.01	1.811	1.90	1.798	1.67	1.753	1.30
1.946	2.20	1.858	1.98	1.854	1.76	1.813	1.17
2.006	2.41	1.911	2.21	1.893	2.21 *	1.858	1.49
2.066	2.45	1.914	2.35 *	1.946	1.57	1.910	1.89 *
		1.983	2.12	2.017	1.62	1.951	1.60 *
		2.061	2.05	2.056	1.66	2.006	1.32
						2.068	1.53

* Too few points to be considered a reliable measurement.

VI. RESULTS AND DISCUSSION

The experimental results are summarized by the plot of $\Delta\alpha/\alpha_{gm}$ vs. T shown in Figure VI. 1. $\Delta\alpha$ is the change in attenuation for a heat flux of 1 Watt/cm^2, i.e., the $q = 1$ intercept values shown in Figures V. 3 to V. 6. The quantity α_{gm} is the attenuation due to mutual friction that would be present for the same heat flux in a channel. Recall that this heat flux must be carried by the normal fluid in the jet. If the superfluid is not entrained by the normal fluid, and if the Gorter-Mellink force is a true volume force which acts in the absence of walls, then α_{gm} should also be the attenuation of second sound in the free jet.

There are several observations that can be made on the basis of Figure VI. 1. The observed attenuation is always less than 8 percent of the Gorter-Mellink attenuation, and α/α_{gm} is clearly temperature dependent with the fraction depending on the distance from the orifice. In addition, the observed $\Delta\alpha$ follows a different power law dependence on the heat flux than α_{gm}. The Gorter-Mellink attenuation is proportional to q^2 while the observed attenuation goes as q^n with $n = 1.3$ to 1.6.

The geometry dependence can be accounted for, to some extent, by spreading of the jet. The spreading would have to be considerably more than has been observed by Kapitza (Ref. 1) and Dimotakis (Ref. 2). Because the length to width ratio of the jet is not large, the ordinary spreading relations for a plane turbulent jet are not entirely applicable, nor are those for an axisymmetric jet. Although all turbulent jets spread linearly with distance, the

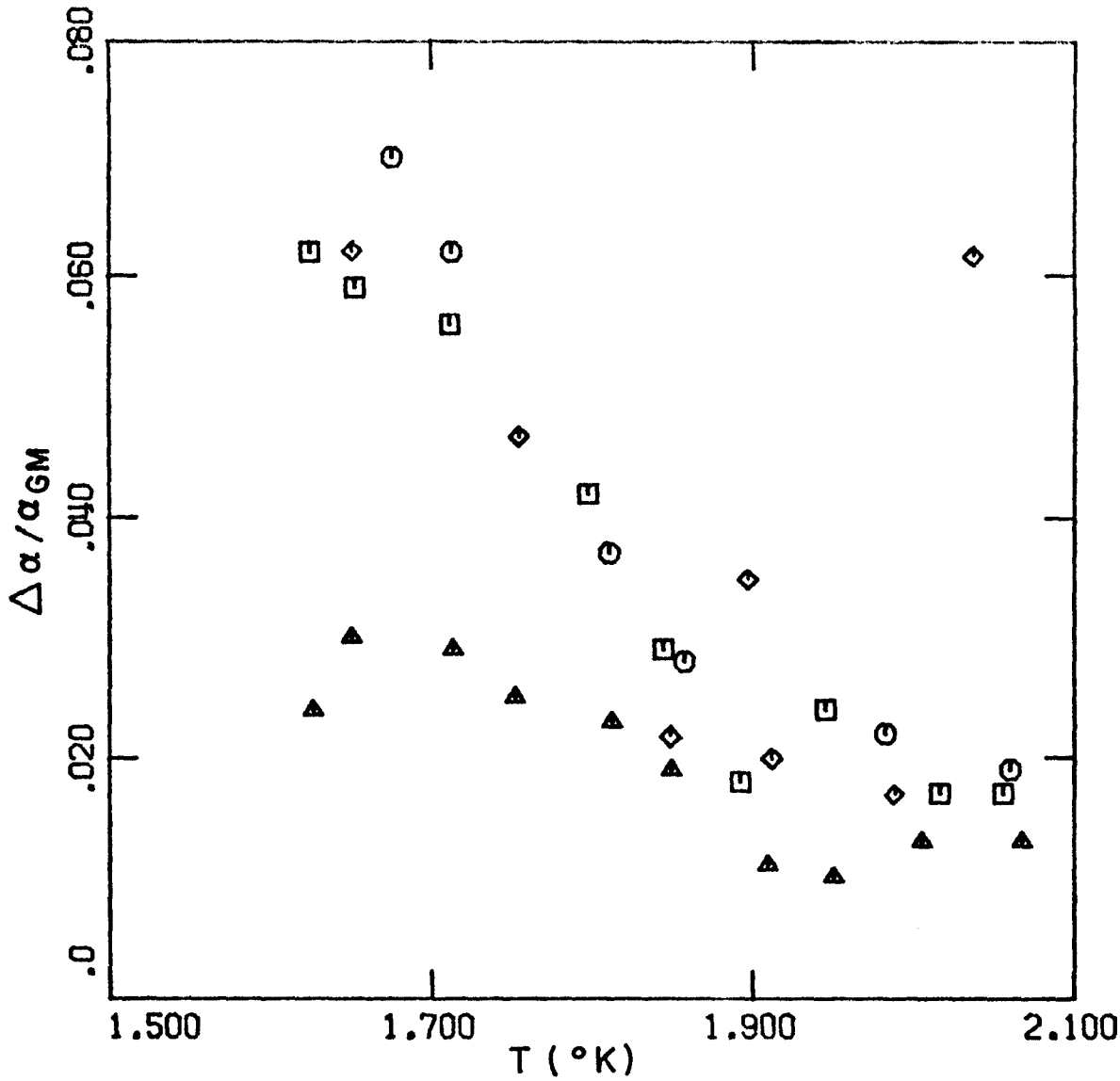

Figure VI. 1. Ratio of the measured attenuation at 1 Watt/cm^2 to attenuation predicted from the mutual friction theory.

angle of spreading depends on the geometry. No geometric scaling can bring the observed attenuation into agreement with the attenuation in a channel because there is already a substantial difference at $x/d = 1/2$ where the jet cannot have spread appreciably. Thus the observed attenuation cannot be due to mutual friction in the sense that this describes the temperature gradient in a channel. However, this conclusion does not shed any new light on how the mutual friction hypothesis is violated. The question of whether the superfluid is entrained by the normal fluid, or whether the Gorter-Mellink force acts only in the presence of walls is still unanswered.

The attenuation results are qualitatively consistent with both the axial gradient measurements of Dimotakis and Broadwell (Ref. 3) and Careri's ion beam attenuation measurements (Ref. 4). Comparatively little attenuation of second sound was observed which would be expected from the lack of temperature gradient in the jet. The fact that some attenuation was observed indicates that the flow in the jet is inhomogenous, thus confirming Careri's observation of ion beam attenuation on the downstream side of his orifice. A further comparison with Careri's data does not seem possible. All of Careri's counterflow measurements were below $1.4^{\circ}K$, and because of the small size of the orifice and low heat flux his Reynolds numbers were always below 1000. In particular, the Reynolds number based on normal fluid density,

$$R_n = \frac{\rho_n d v_n}{\eta}$$

is only 20-30 at these low temperatures, compared with several thousand for the second sound attenuation measurements. It is unclear how to find another dimensionless group to scale the data, or even if one can be found.

It is possible to make a quantitative comparison between the second sound attenuation and temperature gradient measurements. According to the mutual friction theory, the temperature gradient can be related to the attenuation by using the equations

$$\nabla T = b(T)\, q^3 \qquad\qquad \alpha_{gm} = c(T)\, q^2$$

where $b(T)$ is given in Eq. II.13 and $c(T)$ in Eq. II.14 with $q = \rho_s s T w$. One finds that

$$\nabla T = \gamma(T)\, q\, \alpha_{gm} \quad .$$

For comparison, the gradient is computed from the observed attenuation, $\Delta\alpha$, instead of α_{gm}. As a typical example, $\nabla T = 6.66 \times 10^{-4}\ ^{o}K/cm$ for a bath temperature at 1.6^{o}, heat flux of 2.66 Watts/cm^2, and $\Delta\alpha$ measured at 9.6 diameters downstream. This is within the noise level of the carbon thermometer, i.e., such a gradient would be undetectable. The calculation illustrates the increased sensitivity of the second sound attenuation compared to the gradient measurements.

The second sound attenuation in the jet was observed to be frequency independent. If the attenuation is viewed as a scattering process due to inhomogeneities in the flow field, this would indicate

that the second sound wavelength is smaller than the length scale of the inhomogeneities responsible for the scattering. Both Kovasznay (Ref. 5) and Schmidt (Ref. 6) have observed frequency independent scattering of ultrasonic waves in turbulent flows when the wavelength was less than the microscale of the turbulence. This condition is just barely fulfilled in the second sound attenuation experiments, the wavelength being comparable to or slightly less than the microscale. However, in view of the observed frequency independence, a calculation of the attenuation based on geometrical optics is given in Appendix B. This closely follows the calculation for the diffusion of a light (or sound) beam passing through a turbulent boundary layer given by Liepmann (Ref. 7).

REFERENCES

1. P. L. Kapitza, J. Phys. USSR 4, 181 (1941).
2. P. E. Dimotakis, Ph. D. Thesis, California Institute of Technology (1972), page 24.
3. P. E. Dimotakis and J. E. Broadwell, Phys. Fluids 16, 1787 (1973).
4. G. Careri, M. Cerdonio and F. Dupré, Phys. Rev. 167, 233 (1968).
5. Chih-Ming Ho and L. S. G. Kovasznay, Acoustic wave propagation through a two-dimensional turbulent jet, unpublished report (1972).
6. Dieter W. Schmidt, Recent experimental investigations on the scattering of sound by turbulence, AGARD Report 461 (1963).

7. H. W. Liepmann, Deflection and diffusion of a light ray passing through a turbulent boundary layer, Douglas Report SM-14397 (1952).

VII. FUTURE EXPERIMENTS

High frequency second sound has enormous potential as a tool for investigating the flow of liquid helium. It seems almost as if the range of applications is limited only by the imagination of the experimenters. There are three experiments which would be of particular value for understanding the counterflow jet and these will be discussed briefly in this section.

The first set of proposed experiments deals with some refinements of the fluid mechanics of the jet itself. In an ordinary fluid, turbulence quantities and mean velocities do not exhibit self-preservation until many channel diameters downstream. Until the flow is self-preserving the velocity profile of the jet has a memory of the initial velocity distribution which, in turn, is governed by the shape of the pipe or channel producing the jet. After the jet becomes self-preserving, the velocity distributions are independent of the distance from the orifice when nondimensionalized with a suitable local length and velocity scale. It is not practical within the confines of a cryostat to investigate self-preservation. However, considerable improvement in the design of the orifice could be made.

There have been good wind tunnel measurements on the jets produced from long pipes and true orifices. While nothing can substitute for a velocity profile measurement in the liquid helium itself, the ability to draw on classical fluid results would be at least helpful in interpreting attenuation measurements. Some of the uncertainties and assumptions about the flow field could be eliminated.

An unambiguously two-dimensional orifice would also be better for interpretation than the small aspect ratio orifice used in this investigation. The shape used here was an attempt to compromise on several conflicting requirements. The temperature gradient measurements require a wide opening; second sound beam alignment is easier with an elongated opening; and a small area is needed for high heat flux with low total power input. A very narrow slit would make the shape of the orifice unambiguous, and would also increase x/d for a given distance, x, downstream. However, since the attenuation goes as $\exp[-\alpha d]$ there would be a considerable loss in sensitivity if d is made too small.

It may be possible, using second sound, to settle the question of whether the relative velocity W is zero in the counterflow jet. One can show from the linearized equations that second sound propagating in a cavity at an angle to a flow will have a shifted resonant frequency. Specifically, if the mass flow velocity is $\vec{V}$, relative velocity $\vec{W}$, and the resonant frequency of the cavity with $V = W = 0$ is ω_o, then the resonant frequency change will be

$$\Delta\omega = \pm\, \omega_o \left(\frac{\hat{n}\cdot\vec{V}}{2u_2} + f(T)\, \frac{\hat{n}\cdot\vec{W}}{u_2} \right)$$

where

$$f(T) = \frac{u_2^2}{s}\, \frac{\rho_s}{\rho}\, \frac{\partial}{\partial T} \left(\frac{\rho_n}{\rho_s} \right) .$$

The function $f(T)$ goes to zero at about $1.93^{\circ}K$. By working close to this temperature, one should be able to separate the contributions of the mass flow and relative velocities to this frequency

shift. Although V/u_2 and W/u_2 are small, at 100 kHz the change in frequency should be easily within the resolution of the wave analyzer.

For the development of a model of the counterflow jet it is essential to have accurate information about the spreading rate of the jet. The most promising way to obtain this information seems to be schlieren photography. Gulyaev has demonstrated the feasibility of this technique for observing counterflows in liquid helium. His heat fluxes were very high (18-20 Watts/cm^2) but his optical dewar was also homebuilt and not nearly as well adapted to the measurement as the commercially made optical dewars now available in this country. It is hoped to have a working schlieren system at Galcit sometime within the next year for this study.

VIII. CONCLUSION

A technique for the use of high frequency second sound to study the fluid mechanics of liquid helium has been developed and applied to study the additional attenuation of a second sound beam traversing a supercritical counterflow jet. Although the attenuation of the beam was clearly measurable, it was less than 10 percent of that predicted by the mutual friction theory and measured in a counterflow channel. The size of the attenuation is quantitatively consistent with measurements of the temperature gradient in the same jet and with earlier temperature gradient measurements. This once again suggests that either the Gorter-Mellink force acts only in the presence of walls, or the relative velocity is nearly zero in the free jet.

The additional attenuation of second sound by the jet indicates that the flow is inhomogeneous, thus qualitatively confirming earlier investigators' measurements of the ion beam attenuation due to counterflow through an orifice. Frequency independence of the second sound attenuation suggests that the inhomogeneities are larger than the second sound wavelength. The attenuation vs. temperature at various distances downstream from the orifice follow similar, well-defined curves indicating that future experimental and theoretical study is warranted.

APPENDIX A. SECOND SOUND DETECTORS

Several methods have been used for the detection of second sound. Recently, Brillouin scattering (Ref. 1) and stimulated Brillouin scattering (Ref. 2) of laser light have been used. Another novel approach was to make a Helmholtz type resonator using metallized millipore filters (Ref. 3). However, the bolometer still remains the simplest method of second sound observation, and the only one (with the exception of laser scattering) that has the capability of detecting high frequency second sound. The purposes of this appendix are to review some bolometer materials, and to explain the fabrication technique used to produce a bolometer which satisfied the experimental requirements of high frequency second sound detection. The fabrication technique should also be applicable to the hot film velocimeter used for boundary layer studies in ordinary fluids.

A. 1. Types of Resistive Detectors

Any material whose electrical resistance is a strong function of temperature in the liquid helium range is a likely candidate for a second sound balometer. These materials fall naturally into two classes, the semiconductors and superconductors. In a semiconductor the intrinsic carrier concentration, hence the conductivity, is proportional to

$$(kT)^{3/2} \quad \exp\{-E_g/kT\}$$

where E_g is the gap energy (Ref. 4). Consequently, the resistance, R , increases with decreasing temperature, and at liquid

helium temperatures R is so high that doping becomes necessary to make a useful detector. The most often used materials are carbon and germanium. Semiconductor bolometers have the major advantage of excellent sensitivity over the entire liquid helium temperature range. The figure of merit is the slope of the voltage drop versus temperature curve, i.e.,

$$\frac{dV}{dT} = I_o \frac{dR}{dT} \quad ,$$

where I_o is the bias current. Sensitivities up to 1 Volt/^oK can be achieved fairly easily with semiconductors. However, the semiconductor materials also have several disadvantages making them inapplicable to high frequency second sound work. The high resistance makes it difficult to impedance match these detectors to transmission lines. Consequently, they are susceptible to the same noise problems which plagued the old style piezoelectric pressure transducers as well as the 1/f noise characteristic of semiconductors. Electromagnetic crosstalk is also an impedance related problem. The large thermal mass severely limits the frequency response, although with special precautions thin carbon films have been used to detect second sound at frequencies up to 500 kHz (Ref. 5). Since the need to detect second sound at 1 MHz was anticipated, semiconductor detectors were ruled out.

The other commonly used class of bolometer materials is the superconductors. For a superconductor the resistance drops from a high value, R_n , to zero in a small range near the transition temperature, T_c . The principal drawback of the

superconductor is that it has a high sensitivity only over a limited temperature range. This can be overcome by taking advantage of the thermodynamics of superconductors; the transition temperature is a function of the applied magnetic field. The advantages of superconductors are that they have a low resistance reducing both impedance mismatch and crosstalk, and in the form of thin films they have a low thermal mass which gives superconducting thin films the capability of megahertz frequency response. With careful fabrication, sensitivities of 0.6 Volts/^{o}K can be reached; however, an order of magnitude below this is more typical.

Superconducting thin films have been rather extensively studied. Specific application to second sound detection is discussed by Notarys (Ref. 6). Rudnick at UCLA has used an anomalous jump in the transition of granular aluminum films to investigate third sound in liquid helium (Ref. 7). The dV/dT at such a jump is essentially infinite; however, we have been unable to reproduce Rudnick's results.

A.2. Superconducting Thin Film Fabrication Details

The films are made by evaporating a known volume of pure material to completion in a high vacuum. The most convenient way to do this is with a measured length of pure wire. The actual evaporation is done by Joule heating of a molybdenum boat containing the metal sample. The substrate is mounted approximately five inches above the boat. During the evaporation, the pressure was less than 5×10^{-5} torr. Film thickness calibrations were

originally done on an interferometer.

In order to make film with reproducible transition temperatures it was found necessary to keep the heater current and time of evaporation the same. The leads, being thicker, entailed a separate evaporation which had to be done quickly after the first evaporation. Otherwise an oxide layer developed which prevented the leads from making electrical contact.

There are no elemental superconductors with transition temperatures in the working range between $1.3^{\circ}K$ and the λ-point. This necessitates the use of either a compound superconductor or a superposition of superconductor on top of a nonsuperconducting metal. The most satisfactory combination for ease of fabrication and good sensitivity seems to be tin on gold in a 4:1 ratio. A film consisting of 1000 Å of sn on 250 Å of Au characteristically has a normal resistance of 0.5 Ω/square at $4.2^{\circ}K$ and a zero field transition temperature of about $2.1^{\circ}K$. With a suitable magnet, almost the entire temperature range can be covered with one film. A slight change in the ratio of the two metals also changes the transition temperature. Increasing the ratio moves the transition temperature closer to that of the bulk superconductor. This ratio change can best be accomplished by varying the tin thickness because there is a minimum thickness of gold which must be present to be effective. With 250 Å of gold the results were very reproducible. However, with 125 Å of gold and 500 Å of tin the results were not at all consistent and the slope of the transition was considerably degraded.

As mentioned above, the normal resistance of the film is approximately $1/2\Omega$ per square. For impedance matching one wants a resistance at T_c (defined as the temperature where the resistance is $1/2\ R_N$) of 50Ω. Therefore a length-to-width ratio of 200 is necessary. This, plus the requirement of a local measurement, necessitates miniaturization on a scale comparable to thick film hybrid electronic technology. Some compromises in specifications still had to be made, even with a photolithographic technique similar to that used in the manufacture of integrated circuits. This process involves the application of photoresist, a photosensitive plastic coating, over the entire film. The photoresist is then exposed through a contact mask under a mercury vapor ultraviolet light source. Developing removes the exposed portions of the photoresist but leaves a coating of plastic over the unexposed portions which protects that part of the film during the etching process. More detail on the photoresist technique is provided in the next section for future reference. Figure A.1 is a photograph of one of the detectors used in this investigation.

A.3. Photoresist Processing

The photoresist used was Shipley AZ-1350 (manufactured by the Shipley Company Inc., Newton, Mass. 02162). This is a positive working photoresist which means that the exposed portions are removed by the developer. Positive photoresist has the advantage of greater line resolution using a thick photoresist coating than could be achieved with negative working photoresist. The

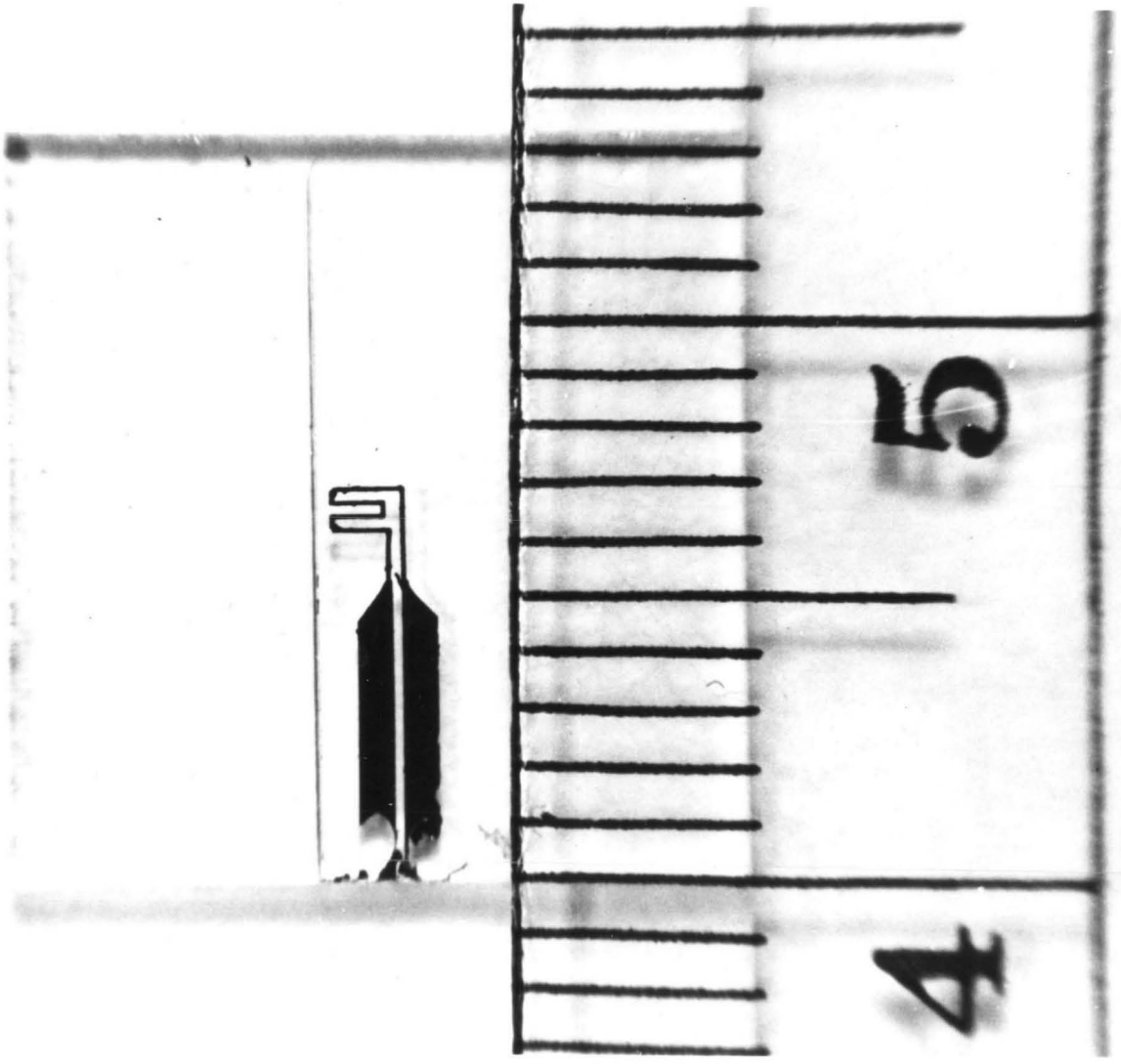

Figure A. 1 A superconducting thin film second sound detector

AZ1350 can be safely handled in gold fluorescent light which is another advantage of positive photoresists. A uniform coating was applied by spinning on a rotating platform at 3000 RPM. The coating was air dried since baking can change the film properties, although baking also makes the photoresist coating more resistant to chemical action.

Exposure of the photoresist is done through a contact mask. This mask is a positive photographic reduction of a pattern either drawn on a white background or laid out on a plastic backing with printed circuit layout tape. Reductions of up to 30:1 are practical at the Caltech graphic arts facility. The emulsion side of the mask must be towards the thin film, and the mask is held flush against the photoresist by a piece of suprasil fused quartz which is transparent to ultraviolet. The exposure time under the mercury vapor lamp is determined by the proximity of the lamp and the size of the pattern. In this application, 15 to 30 seconds was found to be optimum. After exposure, the photoresist is developed for 50 seconds in an aqueous developer (provided by the manufacturer) and rinsed in distilled water. This washes away any photoresist exposed to the uv and leaves a protective coating over the region corresponding to the dark part of the mask. The thin film is now ready for etching.

Of the various etching procedures, chemical etching is the most straightforward. For more accurate work, ion beam etching can be used. Plasma etching and anodization are also accurate

etching techniques but require special materials considerations and are not applicable to gold-tin films. The superimposed tin on gold forms a layer of compounds such as $Au\,Sn_2$ and $Au\,Sn_3$. These are resistant to commonly used chemical etchants, however, a double strength tin etching solution worked reasonably well. Some touching up with a glass needle under a microscope is necessary to complete the process. This was not impractical because of the comparatively large size of the pattern. The tin etch consists of 30 drops HCl + 10 drops HNO_3 + 20 drops H_2O_2 diluted in 30 ml. of ethylene glycol to prevent undercutting. The solution must be cooled for at least 30 minutes before use. Large quantities of the etch cannot be stored because the acid breaks down the solvent in about 1 day. For tin-gold films the amounts of acid and peroxide should be doubled. Etching time is approximately 30 seconds, but this again depends on the size of the pattern, and visual inspection is the only sure method to determine that the etching is completed. Etching for slightly too long undercuts the photoresist and destroys the pattern as does not rinsing promptly and thoroughly in distilled water. It is best to work by successive approximations in short steps.

The photoresist can be removed after etching with reagent grade acetone. This does not leave a residue on the film, and completes the process. With appropriate care and a different exposure and etching technique, half micron lines can be resolved.

REFERENCES

1. R.L. St. Peters, T. J. Greytak and G. B. Benedek, Optics Communications 1, 412 (1970).

2. Dusan Petrac, Ph. D. Thesis, UCLA (1971).

3. R.A. Sherlock and D. O. Edwards, Rev. Sci. Instr. 41, 1603 (1970).

4. Charles Kittel, Introduction to Solid State Physics, (John Wiley & Sons, New York, 1971), 4th ed., Chap. 11, p. 270.

5. H. Snyder, Phys. Fluids 6, 755 (1963)

6. Harris Notarys, Ph. D. Thesis, California Institute of Technology (1964).

7. K. R. Atkins and I. Rudnick, Progr. in Low Temp. Phys. 6 37 (1970).

APPENDIX B

This appendix presents the results of a calculation of the deflection of second sound by a turbulent jet. Many ideas from classical turbulence and their justification in terms of the present experiment will be discussed. While this probably is not a final theoretical answer to what caused the attenuation, the agreement of the calculation with experiment suggests that the basic physical idea may be correct.

B. 1 Some Facts About Turbulent Jets

In a classical fluid, the transition from laminar flow to turbulent flow occurs at a critical value of the Reynolds number

$$R = \frac{\rho v \ell}{\eta}$$

where ℓ is some length scale in the flow. This represents the ratio of inertial to viscous forces. For a classical fluid in a pipe, the critical Reynolds number is 2300, and the jet emerging from the end of such a pipe will always be turbulent.

As a first step, it should be determined whether the counter-flow jet is laminar or turbulent. It is assumed that the relative velocity, w , is zero in the jet but that there is no net mass transfer so v is zero within the confines of the pipe leading to the orifice. Thus in the channel all momentum is associated with the relative motion while in the jet all momentum is carried by v . These momenta must be equal and so conservation of momentum defines the exit velocity. The stagnation point of the superfluid

occurs at or very near to the orifice as indicated by the temperature gradient measurements. Using the equation for the channel

$$w = \frac{q}{\rho_s s T}$$

and the momentum equation, one finds

$$v = \sqrt{\frac{\rho_n}{\rho_s}}\ \frac{q}{\rho s T} \quad .$$

The Reynolds number at the exit is therefore

$$R = \sqrt{\frac{\rho_n}{\rho_s}}\ \frac{q}{s T}\ \frac{d}{\eta}$$

where η is the normal fluid viscosity and d is the diameter of the pipe. Thus the Reynolds number is a strong function of temperature. For a heat flux of 1 Watt/cm^2, R goes from 5400 at 2.1^{o}K to 14,000 at 1.5^{o}K based on the width of the orifice. The jet should be turbulent at all temperatures with a heat flux of .5 Watts/cm^2, however, it may not be turbulent for heat fluxes lower than this at the highest observed temperatures. Since many factors affect the transition, the number R = 2300 should not be taken too literally.

The attenuation at a given temperature, heat flux, and position was observed to be frequency independent. In an ordinary fluid, frequency independent attenuation of sound has been observed when the wavelength is shorter than the microscale of the turbulence. The extent to which this is satisfied will be discussed in a later section, but the observed frequency independence suggests a geometrical optics calculation.

For a plane turbulent jet, the mean velocity profile becomes self-preserving at about 5 diameters downstream. However, the turbulence quantities do not appear to be self-preserving until $x/d = 40\text{-}50$ (Ref. 1). Until the turbulence is self-preserving, the flow has a memory of the nozzle geometry. Even though this calculation is concerned with $x/d < 20$ it will be assumed that the small scale of turbulence has reached its asymptotic state of local isotropy.

B. 2. Mean Square Deflection Angle

The most important part of the calculation is based on an argument due to Liepmann (Ref. 2) for the mean square deflection of a light beam passing through a turbulent boundary layer, under the condition that the wavelength is much smaller than the correlation length. Let x be the streamwise direction, y the cross stream direction and let the thickness of the boundary layer be δ. The index of refraction is in the form $n = n_o(y)\ (1 + n')$, with $n' << 1$ representing the random fluctuating part of the index of refraction due to the turbulence, $\overline{n'} = 0$ (overbars indicate time averaging).

Light rays are assumed to enter the boundary layer in the normal direction. Therefore, spreading of the jet over the dimensions of the beam is ignored. In the experiment, the part of the beam of interest is only 1 mm so this should be a good approximation.

Liepmann's result for the mean square angle of deflection is

$$\overline{\epsilon^2}(\delta) = \frac{2}{n_o^2(\delta)} \iint_o^\delta n_o(y)\, n_o(\xi) \overline{\left(\frac{\partial n'}{\partial x}\right)^2} R(|y - \xi|)\, dy\, d\xi$$

provided that the fluctuations are homogeneous over regions larger than the correlation length. R is a correlation function, i.e.,

$$\overline{\left(\frac{\partial n'}{\partial x}\right)_y \left(\frac{\partial n'}{\partial x}\right)_\xi} = \overline{\left(\frac{\partial n'}{\partial x}\right)^2} R(|y - \xi|) \quad .$$

B. 3. Index of Refraction of Second Sound

Khalatnikov (Ref. 3) has shown that for second sound in the presence of a flow,

$$u_2 = u_{20} + v_y + \gamma w_y$$

where v_y and w_y are the components of the mass flow and relative velocities in the direction of the second sound propagation. γ is a monotonically decreasing function of temperature. For the jet, w_y is taken to be zero. The calculation has been tried with $v_y = 0$, $w_y \neq 0$ but a different temperature dependence results. The index of refraction is

$$n = \frac{u_{20}}{u_2} = 1 - \frac{v_y}{u_2} \quad .$$

Let $v_y = \tilde{v}_y + v_y'$ where $\tilde{v}_y$ is the mean velocity and v_y' is the turbulence component, i.e., $\overline{v_y'} = 0$. The index of refraction can now be written in the form

$$n = \left(\frac{\tilde{v}_y}{u_{20}}\right)\left(1 - \frac{v_y'}{u_{20}}\right) \quad .$$

B. 4. Correlation Length

It will become necessary to choose a correlation length to complete the calculation. Dimotakis (Ref. 4) has suggested a dimensionless group to scale the onset of mutual friction in a channel. For a critical heat flux q_c, the relation

$$\frac{A q_c \ell}{sT} = 1$$

seems to hold where ℓ is the channel diameter and A is the coefficient in the force of mutual friction. The correlation length proposed here is

$$\frac{1}{\Lambda} = c \frac{Aq}{sT}$$

where c is a number of order unity.

B. 5. Completion of the Calculation

For the jet, δ is outside the region of high velocity so one can reasonably take $n_o(\delta) = 1$. If the correlation function falls to zero rapidly for increasing $|y - \xi|$ then one can replace $R(|y - \xi|)$ with $\Lambda\delta(|y - \xi|)$ where Λ is the scale of fluctuations and $\delta(|y - \xi|)$ is the Dirac δ-function.

$$\overline{e^2}(\delta) = 2\Lambda \int_o^\delta n_o^2(y) \overline{\left(\frac{\partial n'}{\partial x}\right)^2} \, dy \quad .$$

We now use the mean value theorem and approximate the averages separately, i.e.,

$$(n_o^2)_{ave} = 1$$

$$\overline{\left(\frac{\partial n'}{\partial x}\right)^2}_{ave} \simeq \frac{\overline{n'^2}}{\lambda^2}$$

where λ is the microscale. The microscale will be approximately the correlation length so that

$$\overline{\epsilon^2(\delta)} = 2\,\frac{\delta}{\Lambda}\,\frac{\overline{(v_y')^2}}{u_{20}^2} \quad .$$

For $\overline{(v_y')^2}$ the experimentally determined relations for an ordinary plane turbulent jet will be used.

$$\overline{(v_y')^2} \simeq .078\ U_s^2$$

where U_s is the mean center line velocity (Ref. 1) given by the formula

$$U_s = U_J \left(\frac{d}{x}\right)^{\frac{1}{2}} \quad .$$

U_J is the exit speed of the jet (Ref. 5).

$$\overline{\epsilon^2(\delta)} = 0.156\,\frac{\delta}{\Lambda}\,\frac{d}{x}\left(\frac{U_J}{u_{20}}\right)^2 \quad .$$

B. 6. Conclusion

The attenuation is related to the mean square deflection by the formula

$$\alpha = \frac{2\sqrt{\overline{\epsilon^2}}}{\mathcal{L}}$$

where $\mathcal{L}$ is the size of the beam. Finally, we get after substitutions for Λ and U_j

$$\alpha = \frac{f(T,\delta)}{\mathcal{L}}\, q^{3/2} \quad .$$

Note that δ, the width of the jet, is a function of the distance downstream from the orifice. The function $\frac{f(T,\delta)}{\mathcal{L}}$ is plotted in Figure B.1 for a position 20 diameters from the jet exit. The constant in Λ has been chosen to be 1/3.

It is necessary to examine the assumption that Λ is greater than the wavelength. With the above choice of the constant, Λ ranges from 0.18 to 0.41 mm while the second sound wavelength goes from 0.2 to 0.15 mm for a 100 kHz frequency in the temperature range 1.50 to 2.05°K. Thus the condition on the coherence length is at least approximately satisfied.

The result of this calculation is extremely suggestive and the following things may be inferred:

1) The superfluid must move with the normal fluid. Using a relative velocity instead of v gives the wrong temperature dependence.

2) The jet is turbulent. A laminar profile cannot give attenuation of the magnitude observed. Using the spreading relations for a turbulent jet removes most of the geometry dependence of the attenuation.

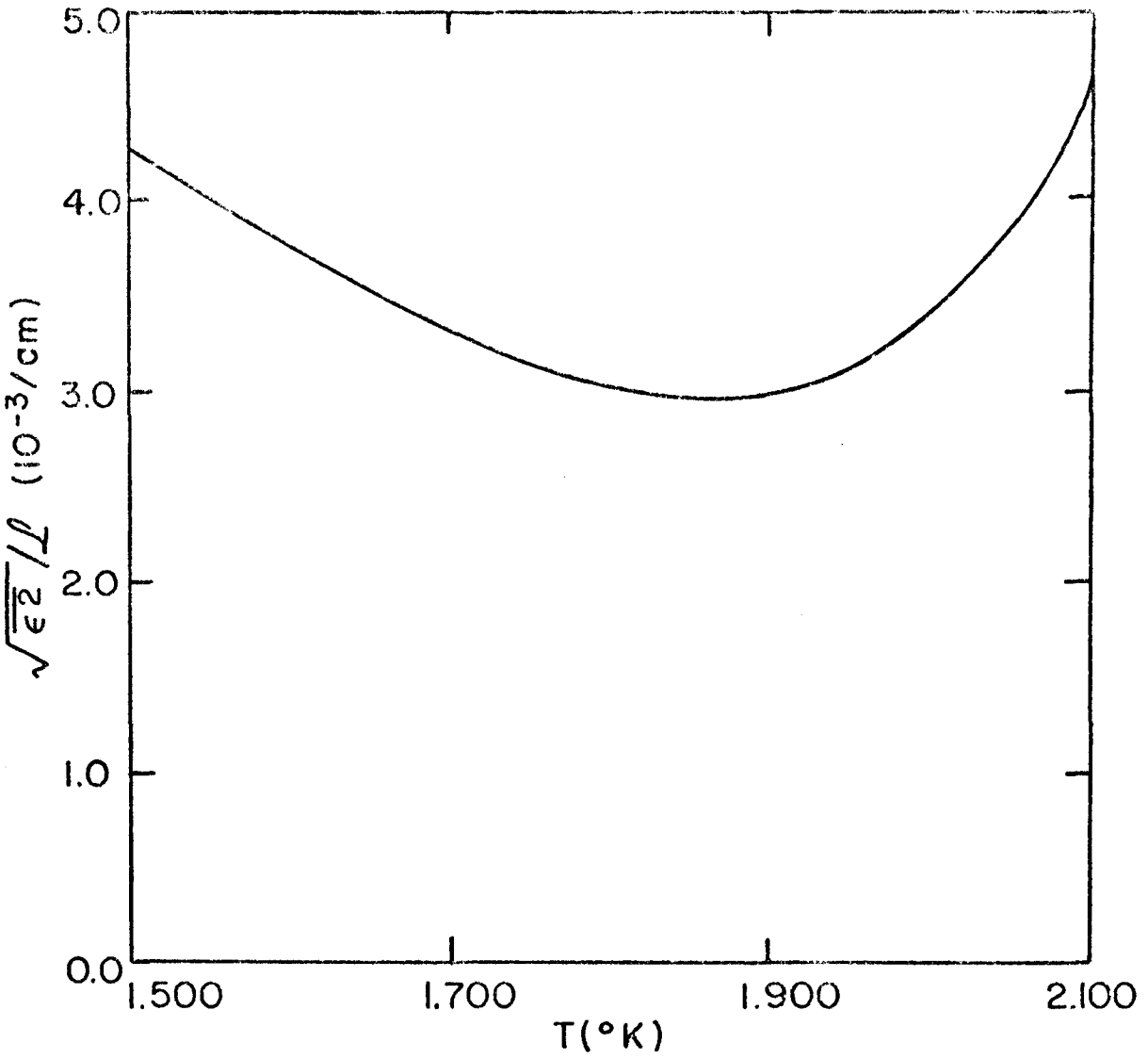

Figure B. 1. Attenuation calculated from the mean square deflection angle.

3) The coherence length in the jet is the Gorter-Mellink length scale. This suggests that the mutual friction acts away from solid boundaries but in a previously unsuspected way. Mutual friction, as a source of entropy, assumes a role something like viscous dissipation in an ordinary fluid.

REFERENCES

1. H. Tennekes and J.L. Lumley, A First Course in Turbulence, (MIT Press, Cambridge, 1972), page 130.
2. H.W. Liepmann, Deflection and diffusion of a light ray passing through a boundary layer, Douglas Report SM-14397 (1952).
3. I.M. Khalatnikov, Sov. Phys. -JETP 3, 649 (1956).
4. P.E. Dimotakis, Phys. Rev. A10, 1721 (1974).
5. H. Schlichting, Boundary-Layer Theory, (McGraw-Hill Book Co., New York, 1968), page 697.